

Supporting Information

A Non-alternant Aromatic Belt: Methylene-bridged [6]Cycloparaphenylene Synthesized from Pillar[6]arene

Yuanming Li,[†] Yasutomo Segawa,^{‡, #, §, \$} Akiko Yagi,[‡] and Kenichiro Itami^{*, †, ‡, #}

[†]Institute of Transformative Bio-Molecules (WPI-ITbM), Nagoya University, Chikusa, Nagoya 464-8602, Japan

[‡]Graduate School of Science, Nagoya University, Chikusa, Nagoya 464-8602, Japan

[#]JST-ERATO, Itami Molecular Nanocarbon Project, Nagoya University, Chikusa, Nagoya 464-8602, Japan

[§]Institute for Molecular Science, Myodaiji, Okazaki, 444-8787, Japan

^{\$}Department of Structural Molecular Science, SOKENDAI (The Graduate University for Advanced Studies), Myodaiji, Okazaki, 444-8787, Japan.

****E-mail: itami@chem.nagoya-u.ac.jp (K.I.).***

Table of Contents

1. General.....	S3
2. The synthesis of methylene-bridged [6]CPP	S4
2.1 The synthesis of pillar[6]arene.....	S4
2.2 The synthesis of hydroxylated pillar[6]arene	S5
2.3 The synthesis of triflate-functionalized pillar[6]arene.....	S6
2.4 The synthesis of methylene-bridged [6]CPP	S7
2.5 The optimization of intramolecular nickel-mediated Yamamoto coupling	S8
3. The X-ray crystal structure	S9
3.1 The comparison of X-ray crystal structure and DFT calculated result	S10
3.2 The CH– π distances between methylene-bridged [6]CPPs	S11
3.3 The reduction of length of LPP	S12
4. Computational study	S14
4.1 HOMO and LUMO energies of [n]CPP, CH ₂ -bridged [n]CPP, and [n]LPP.....	S14
4.2 Optimized structures and frontier molecular orbitals	S16
4.3 The calculation of strain energy	S36
4.4 Simulated NMR chemical shifts (ppm)	S38
4.5 TD-DFT vertical one-electron excitations	S39
4.6 Uncorrected and thermal-corrected energies of stationary points	S41
4.7 Cartesian coordinates of optimized structures	S42
5. Photophysical properties and stability test.....	S42
6. Representative aromatic belts having CPP skeleton.....	S43
7. Comparison among 4 , [6]CPP, [6,6]CNCB, and pillar[6]arene	S44
8. NMR spectra of new compounds.....	S45
9. References.....	S51

1. General

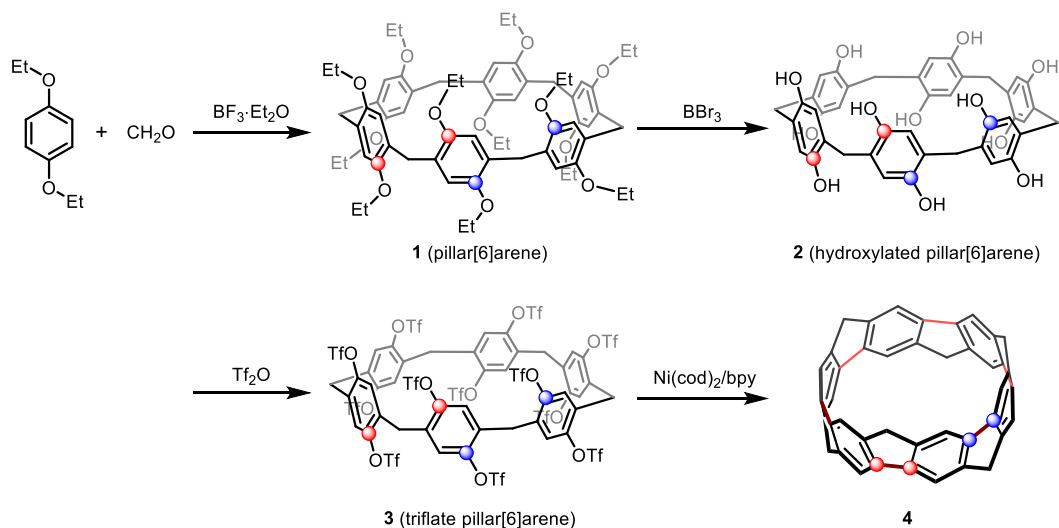
Unless otherwise noted, all reactants or reagents including dry solvents were obtained from commercial suppliers and used as received. Unless otherwise noted, all reactions were performed with dry solvents under an atmosphere of argon in dried glassware using standard vacuum-line techniques. All work-up and purification procedures were carried out with reagent-grade solvents in air.

Analytical thin-layer chromatography (TLC) was performed using E. Merck silica gel 60 F254 precoated plates (0.25 mm); detection with UV light or by dipping into a solution of KMnO_4 (1.5 g in 400 mL H_2O , 5 g NaHCO_3), followed by heating. Flash column chromatography was performed with E. Merck silica gel 60 (230-400 mesh). The developed chromatogram was analyzed by a UV lamp (254 nm). Medium pressure liquid chromatography (MPLC) was performed using Yamazen W-prep 2XY. Preparative thin-layer chromatography (PTLC) was performed using Wakogel B5-F silica-coated plates (0.75 mm) prepared in our laboratory. Preparative gel permeation chromatography (GPC) was performed with a JAI LC-9204 instrument equipped with JAIGEL-1H/JAIGEL-2H columns using chloroform as an eluent. Gas chromatography (GC) analysis was conducted on a Shimadzu GC-2010 instrument equipped with a HP-5 column (30 m \cdot 0.25 mm, Hewlett-Packard) with dodecane as an internal standard.

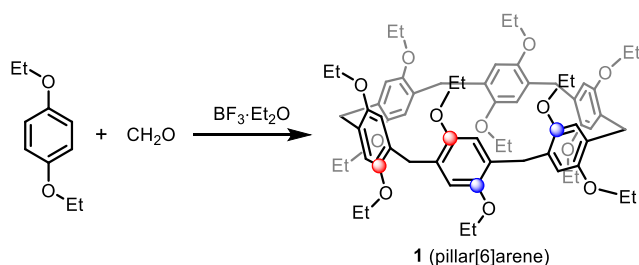
The high-resolution mass spectra (HRMS) were conducted on Thermo Fisher Scientific Exactive. Infrared spectra were recorded on a JASCO FTIR-6100 spectrometer. Nuclear magnetic resonance (NMR) spectra were recorded on a JEOLJNM-ECA-600 (^1H 600 MHz, ^{13}C 150 MHz) spectrometer and a JEOL JNM-ECA-400 (^1H 400 MHz, ^{13}C 100 MHz) spectrometer. Chemical shifts for ^1H NMR are expressed in parts per million (ppm) relative to tetramethylsilane (δ 0.00 ppm) or residual peak of CDCl_3 (δ 7.26 ppm). Chemical shifts for ^{13}C NMR are expressed in ppm relative to CDCl_3 (δ 77.16 ppm) or acetone- d_6 (δ 29.84 ppm). Chemical shifts for ^{19}F NMR are expressed in ppm relative to C_6F_6 (δ -164.9 ppm). Data are reported as follows: chemical shift, multiplicity (s = singlet, d = doublet, dd = doublet of doublets, t = triplet, m = multiplet, brs = broad singlet), coupling constant (Hz), and integration.

2. The synthesis of methylene-bridged [6]CPP

Scheme S1. The synthetic route leading to methylene-bridged [6]CPP.

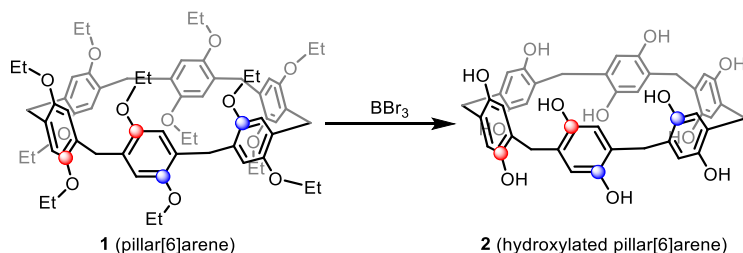


2.1 The synthesis of pillar[6]arene



In 2009, pillar[6]arene was first synthesized by Cao and coworker.¹ Although many high-yield synthetic methods were reported recently, the synthesis of pillar[6]arene from 1,4-diethoxybenzene and paraformaldehyde using $\text{BF}_3 \cdot \text{Et}_2\text{O}$ as a catalyst is still attractive,² due to the easily accessible starting materials and applicable to large-scale synthesis. The mixture of 1,4-diethoxybenzene (6.15 g, 37.0 mmol, 1.0 equiv) and paraformaldehyde (1.33 g, 44.4 mmol, 1.2 equiv) in anhydrous CHCl_3 (300 mL) was stirred at 30 °C under nitrogen for 0.5 h, followed by dropwise addition of $\text{BF}_3 \cdot \text{Et}_2\text{O}$ (5.9 mL, 48.1 mmol, 1.2 equiv). (Temperature is crucial for the reaction). After being stirred for 1 h at 30 °C, a dark green solution was obtained. And the reaction solution was washed with brine (100 mL). The organic layers were dried over anhydrous Na_2SO_4 , filtered and concentrated by rotary evaporation. The residue was then purified by silica gel column chromatography with gradient elution of *n*-hexane/EtOAc/ CH_2Cl_2 (25:1:1→5:1:1) to give **1** (pillar[6]arene) (470 mg, 0.44 mmol, 7.0%, white solid) and pillar[5]arene (1.9 g, 2.1 mmol, white solid). R_f (EtOAc/hexane = 1:10): 0.4 (pillar[5]arene) and 0.2 (pillar[6]arene); ^1H and ^{13}C NMR spectra are consistent with the previous report.² ^1H NMR (CDCl_3 , 400 MHz): δ 6.69 (s, 12H), 3.83 (q, J = 6.4 Hz, 24H), 3.79 (s, 12H), 1.28 (t, J = 6.4 Hz, 36H).

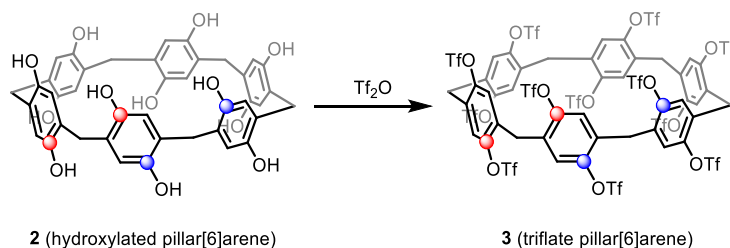
2.2 The synthesis of hydroxylated pillar[6]arene³



To a solution of pillar[6]arene (1.05 g, 982 μmol , 1.0 equiv) in dry CHCl_3 (40 mL) was added BBr_3 (39.3 mL, 39.3 mmol, 40 equiv, 1 M in dichloromethane) dropwise at 0 $^\circ\text{C}$. After the addition, the mixture was warmed slowly to room temperature and stirred for 24 h. After the reaction, MeOH (1 mL) was added very slowly at 0 $^\circ\text{C}$ and followed by ice water (10 mL). (The quenching of BBr_3 fumes violently!) And the precipitate was collected by filtration and washed with copious amounts of 0.5 M aqueous hydrochloric acid, water, and chloroform.

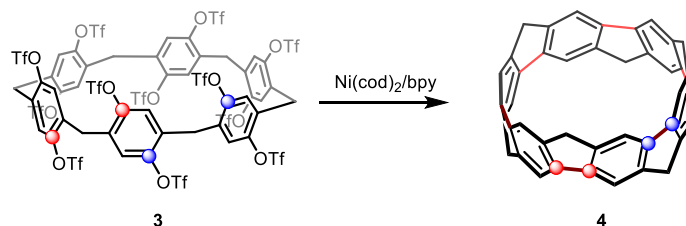
Subsequently, the precipitate was dissolved in acetone, dried over Na_2SO_4 , and filtered. CHCl_3 (50 mL) was added to the resulting acetone solution. The mixture was concentrated until about 10 mL of the solution remained, 100 mL CHCl_3 was further added slowly. The resulting precipitate was collected and dried under high vacuum to give **2** (630 mg, 0.86 mmol, 88%) as a light pink solid without further purification (keep the compound in a fridge). R_f ($\text{CH}_2\text{Cl}_2/\text{MeOH} = 10:1$): 0.3; ^1H and ^{13}C NMR spectra are consistent with the previous report.³ ^1H NMR (acetone- d_6 , 400 MHz): δ 7.71 (s, OH), 6.55 (s, 12H), 3.65 (s, 12H). ^1H NMR (acetone- d_6 /1 drop D_2O , 400 MHz): δ 6.54 (s, 12H), 3.66 (s, 12H).

2.3 The synthesis of triflate-functionalized pillar[6]arene⁴



To a solution of hydroxylated pillar[6]arene (491 mg, 670 μmol , 1.0 equiv) in CH_2Cl_2 (90 mL), pyridine (0.97 mL, 12 mmol, 18 equiv) and trifluoromethanesulfonic anhydride (1.8 mL, 10.7 mmol, 16 equiv) were added at 0 $^\circ\text{C}$ under N_2 atmosphere. (Hydroxylated pillar[6]arene could not totally dissolve in CH_2Cl_2 .) After addition, a large amount of precipitate was formed. The mixture was warmed slowly to room temperature and stirred for 24 hours. After the reaction, water (10 mL) was added at 0 $^\circ\text{C}$ slowly. The reaction mixture was concentrated until about 20 mL amount of CH_2Cl_2 remained. And the precipitate was collected by filtration, washed with copious amounts of water, and 10 mL solution of *n*-hexane/ CH_2Cl_2 (1:1), followed by drying under high vacuum. Subsequently, the solid was dissolved with acetone and purified by a short column of silica with gradient elution of acetone/hexane (1:1 \rightarrow 1:0). The solution was concentrated until about 5 mL of the solution remained, 50 mL *n*-hexane was further added slowly. The resulting precipitate was collected to give triflate-functionalized pillar[6]arene **3** (1.05 g, 453 μmol , 68%) as a white solid. R_f (*n*-hexane/acetone = 5:1): 0.5; ^1H NMR (600 MHz, acetone- d_6) δ 7.51 (s, 12H), 4.47 (s, 12H). ^{19}F NMR (369 MHz, acetone- d_6) δ -74.88. ^{13}C NMR (150 MHz, acetone- d_6) δ 147.5, 133.5, 126.2, 119.3 (q, $J_{\text{FC}} = 320$ Hz), 30.9. HRMS (ESI): Exact mass calculated for $\text{C}_{54}\text{H}_{24}\text{F}_{36}\text{NaO}_{36}\text{S}_{12}$ ($[\text{M}+\text{Na}]^+$): 2338.6013, mass found: 2338.6089.

2.4 The synthesis of methylene-bridged [6]CPP



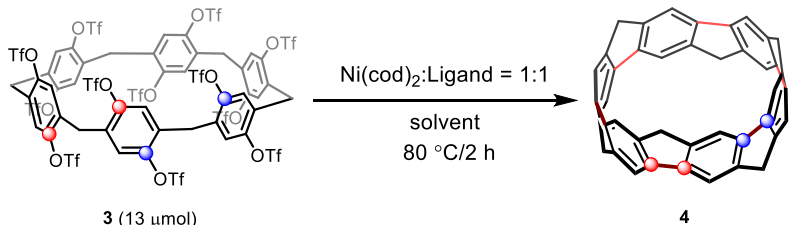
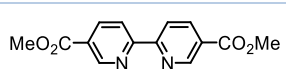
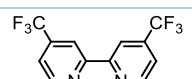
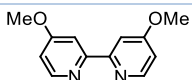
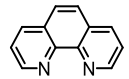
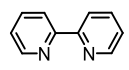
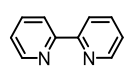
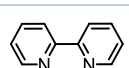
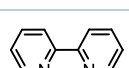
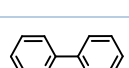
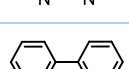
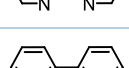
To a dry Schlenk tube charged with 2,2'-bipyridyl (84.3 mg, 540 μ mol, 12 equiv), was added Ni(cod)₂ (148 mg, 540 μ mol, 12 equiv) under argon (this operation in the glovebox), followed by *N*-methyl-2-pyrrolidone (NMP) (6.0 mL). The mixture was stirred for 40 mins at room temperature and a dark purple solution of the complex was obtained quickly (about 3 mins later). The mixture was set in an oil bath at 80 °C and stir for 5 mins to reach thermal equilibrium and complete the formation of the nickel complex. The solution of pillar[6]arene triflate **3** (104 mg, 45.0 μ mol, 1.0 equiv) in NMP (9.0 mL) was then added in one portion. After 2 hours of stirring at 80 °C, the reaction mixture was allowed to cool down to rt, then diluted with CH₂Cl₂ (30 mL) and sat. aq. NH₄Cl (30 mL).

The dark purple heterogeneous mixture was vigorously stirred for 10 mins. The organic layer was separated and then *n*-hexane (60 mL) was added. The organic layer was further washed once with sat. aq. NH₄Cl (30 mL), two-time with water (2×30 mL) and one-time with brine (30 mL). Subsequently, the organic layer was dried over Na₂SO₄, filtered. The solution was concentrated until about 5 mL of the solution remained by rotary evaporation at rt. The resulting precipitate was collected, and then purified by a short (2 cm long) silica gel column chromatography quickly with CH₂Cl₂/*n*-hexane/CS₂ (25:50:2) as eluent. The red fractions were concentrated under rotary evaporation and dried under high vacuum for more than 20 mins. Subsequently, *n*-hexane/CHCl₃ (6:1) was added in the flask and then decanted for several times until the solution of *n*-hexane/CHCl₃ become colorless. The red solid on the flask wall was dried to give the target compound **4** (4.2 mg, 7.9 μ mol, 18%). (The pure product is practically insoluble in CHCl₃, less than 1 mg/10 mL.) R_f (*n*-hexane/CH₂Cl₂/CS₂ = 20:10:1): 0.4 (Without CS₂, the product could not be observed on TLC.). ¹H NMR (600 MHz, CD₂Cl₂) δ 7.88 (s, 12H), 4.27 (d, *J* = 17.5 Hz, 6H), 4.01 (d, *J* = 17.5 Hz, 6H). ¹³C NMR (150 MHz, CD₂Cl₂) δ 149.0, 137.7, 122.4, 41.2. ¹H NMR (600 MHz, CDCl₃) δ 7.86 (s, 12H), 4.29 (d, *J* = 17.0 Hz, 6H), 4.09 (d, *J* = 17.0 Hz, 6H). HRMS (ESI): Exact mass calculated for C₄₂H₂₅ ([M+H]⁺): 529.1951, mass found: 529.1902. (See Figure S27 for the photostability data.)

Note of purification by silica gel column chromatography: (1) Before purification by column, the silica gel column should be washed with CH₂Cl₂/*n*-hexane/CS₂ (25:50:2). (2) The precipitate (crude product) was dissolved by CH₂Cl₂/*n*-hexane/CS₂ (25:50:2, 1 mL), and then transfer to the top of the column directly.

2.5 The optimization of intramolecular nickel-mediated Yamamoto coupling

Table S1. The optimization of intramolecular nickel-mediated aryl-aryl coupling.^a

 <p style="text-align: center;">3 (13 μmol) 4</p>			
entry	ligand	solvent (mM) ^b	4 (%) ^c
1		DMA (4.3)	3.0
2		DMA (4.3)	6.9
3		DMA (4.3)	3.8
4		DMA (4.3)	1.3
5		DMA (4.3)	13
6^d		DMA (4.3)	n.d.
7		DMA/toluene = 2:1 (4.3)	9.4
8		NMP (4.3)	19 (15)
9		NMP (1.5)	18
10		NMP (3.0)	20 (15)
11		NMP (6.0)	17

^a**3** (13 μ mol), Ni(cod)₂ (12 equiv), ligand (12 equiv), 80 °C, 2 h. ^bThe concentration of **3** in the solvent. ^c¹H NMR yield using CH₂Br₂ as the internal standard. Isolated yields are shown in parentheses. ^dNo preformation of the Ni(cod)₂/2,2'-bipyridyl complex.

3. The X-ray crystal structure

Details of the crystal data and a summary of the intensity data collection parameters are listed in Table S2. A suitable crystal was mounted with mineral oil on a MiTeGen MicroMounts and transferred to the goniometer of the kappa goniometer of a RIGAKU XtaLAB Synergy-S system with 1.2 kW MicroMax-007HF microfocus rotating anode (Graphite-monochromated Mo K α radiation ($\lambda = 0.71073$ Å)) and PILATUS200K hybrid photon-counting detector. Cell parameters were determined and refined, and raw frame data were integrated using CrysAlisPro (Agilent Technologies, 2010). The structures were solved by direct methods with SHELXT⁵ and refined by full-matrix least-squares techniques against F^2 (SHELXL-2018/3)⁶ by using Olex2 software package.⁷ The intensities were corrected for Lorentz and polarization effects. The non-hydrogen atoms were refined anisotropically. Hydrogen atoms were placed using AFIX instructions. CCDC 2007092 contains the supplementary crystallographic data for this paper. These data can be obtained free of charge from The Cambridge Crystallographic Data Centre via www.ccdc.cam.ac.uk/data_request/cif.

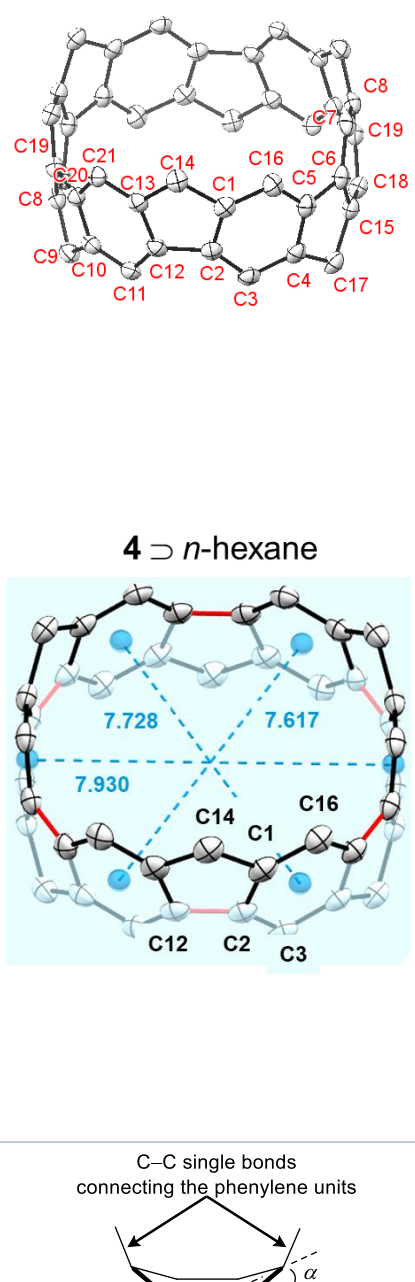
Table S2. Crystallographic data and structure refinement details for **4**.

	4		
formula	C _{45.5} H ₃₂ Cl	V (Å ³)	1530.71(6)
fw	614.16	Z	2
T (K)	123(2)	D_{calc} (g/cm ³)	1.333
λ (Å)	0.71073	μ (mm ⁻¹)	0.160
cryst syst	Triclinic	$F(000)$	644.0
space group	$P-1$	cryst size (mm)	0.15 \times 0.10 \times 0.10
a (Å)	11.4850(3)	2θ range (deg)	3.53 to 55.768
b (Å)	11.7900(3)	reflns collected	18175
c (Å)	12.1794(3)	indep reflns/ R_{int}	6100/0.0444
α (deg)	107.588(2)	params	460
β (deg)	92.5269(19)	GOF on F^2	1.056
γ (deg)	101.5278(19)	R_1, wR_2 [$I > 2\sigma(I)$]	0.0582, 0.1543
		R_1, wR_2 (all data)	0.0903, 0.1702

3.1 The comparison of X-ray crystal structure and DFT calculated result

The optimization of the structure of compound **4** was carried out by DFT calculations at the B3LYP/6-31G(d) level of theory, and the calculated optimized structure reproduced the experimentally observed structure well.

Table S3. The comparison of the X-ray crystal structure and DFT calculated result.

Bond length (Å) (4 \supset <i>n</i> -hexane)				
	Bond	Observed	Averaged	Calculated
	C1–C2	1.408(3)	1.408	1.416
	C12–C13	1.405(3)		
	C20–C10	1.409(3)		
	C19–C8	1.412(3)		
	C15–C6	1.410(3)		
	C4–C5	1.406(3)		
	C1–C14	1.512(3)	1.518	1.521
	C13–C14	1.519(3)		
	C9–C10	1.521(3)		
	C8–C9	1.518(3)		
	C4–C17	1.519(3)		
	C17–C15	1.520(3)		
	C2–C12	1.475(3)	1.478	1.478
	C19–C20	1.474(3)		
	C6–C5	1.485(3)		
	C11–C12	1.393(3)	1.395	1.404
	C20–C21	1.395(3)		
	C2–C3	1.403(3)		
	C16–C5	1.389(3)		
	C6–C7	1.397(3)		
	C18–C19	1.395(3)		
	C21–C13	1.384(3)	1.384	1.391
	C10–C11	1.380(3)		
	C1–C16	1.390(3)		
	C3–C4	1.383(3)		
	C15–C18	1.383(3)		
	C7–C8	1.383(3)		
	Diameter		7.758	7.759
	Bent angle α	9.08, 9.51 8.54, 8.60 7.79, 7.04	8.43	—

3.2 The CH- π^{centroid} distances between methylene-bridged [6]CPPs

There is no clear intermolecular π - π interaction was observed. Instead, close CH- π^{centroid} interactions were observed.

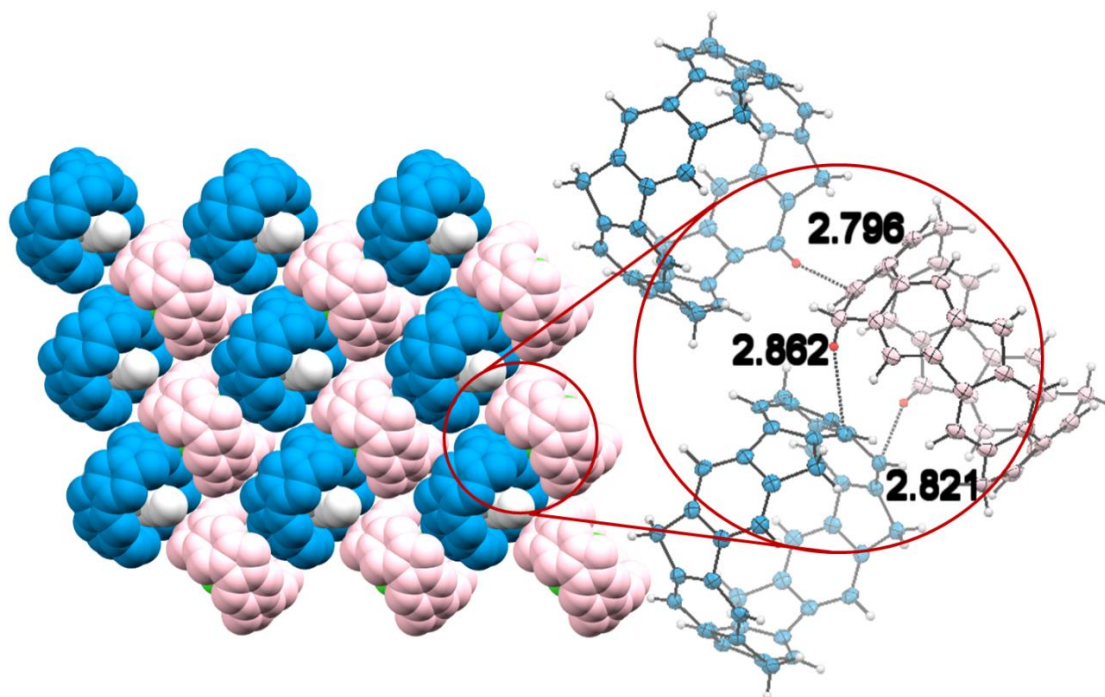
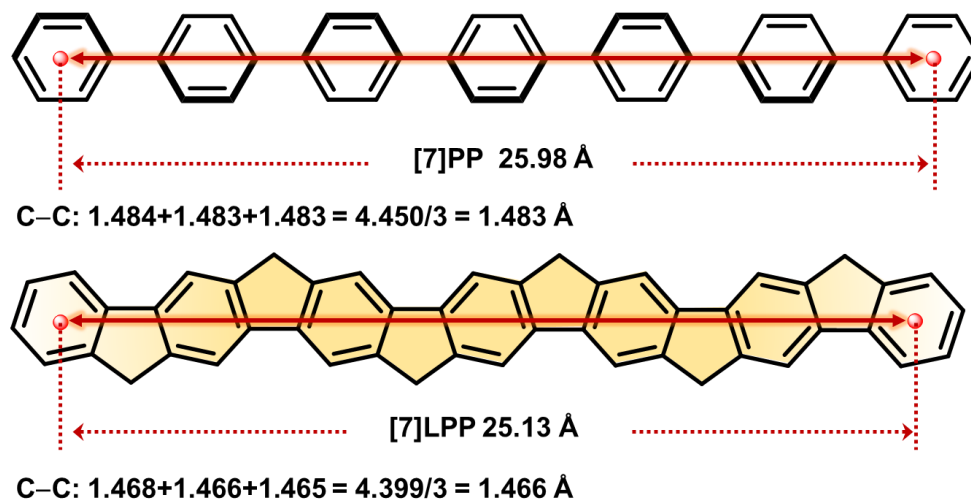


Figure S1: Packing structure of **4** (the $[0\bar{1}1]$ plane) (**4** (blue) \supset *n*-hexane (grey); **4** (pink) \supset CH₂Cl₂ (green)). View of the X-ray crystal structures and the CH- π distances.

3.3 The reduction of length of LPP

The phenylene units of linear paraphenylenes linked with methylene bridges forms the condensed ladder-type paraphenylenes (LPPs) with shorter length (25.98 Å vs 25.13 Å). This result is consistent with the reduction of the diameter of **4** compared to the diameter of [6]CPP.



$25.98 - 25.13 = 0.86 \text{ \AA}$ (This length difference come from two reasons.)

(1) The shortness of six C–C single bonds: $1.483 - 1.466 = 0.017 \times 6 = 0.10 \text{ \AA}$

(2) The major reason is the different alignment of phenylene units: $0.86 - 0.10 = 0.76 \text{ \AA}$

Figure S2. The optimized structures of [7]PP and [7]LPP were calculated at the B3LYP/6-31G(d) level of theory.

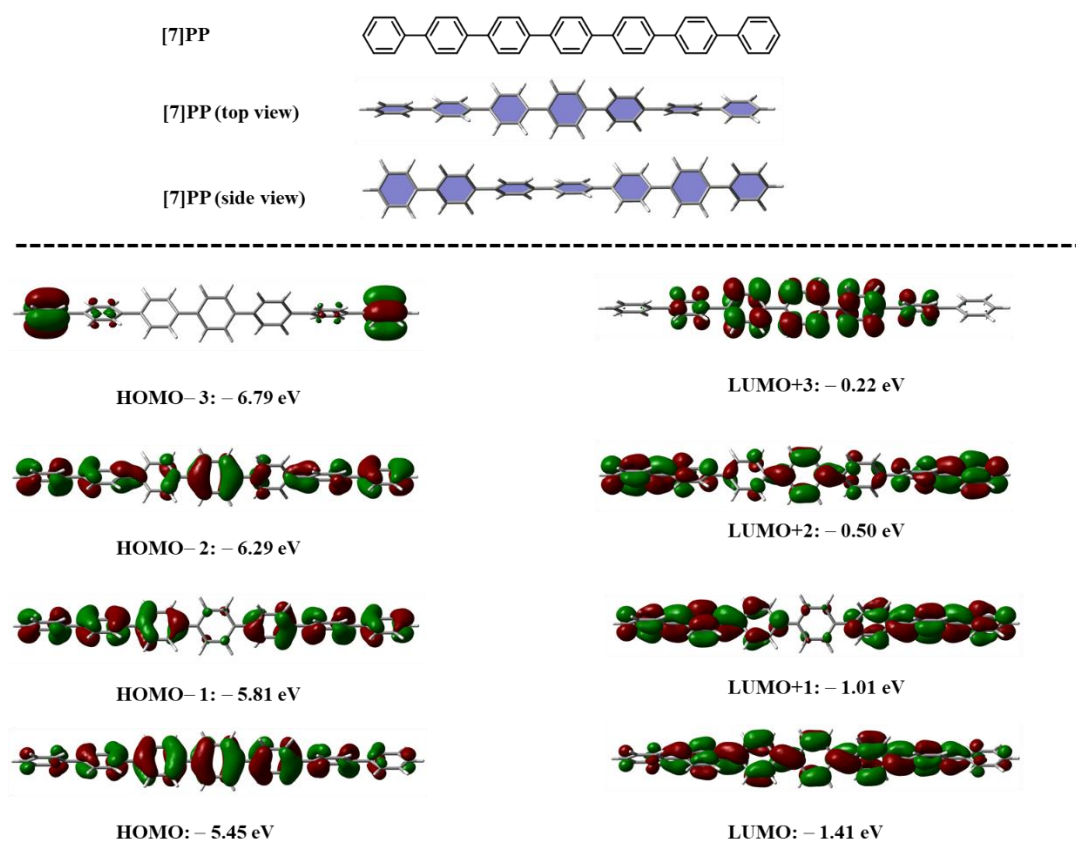


Figure S3. The frontier orbital energies of [7]PP calculated by B3LYP/6-31G(d).

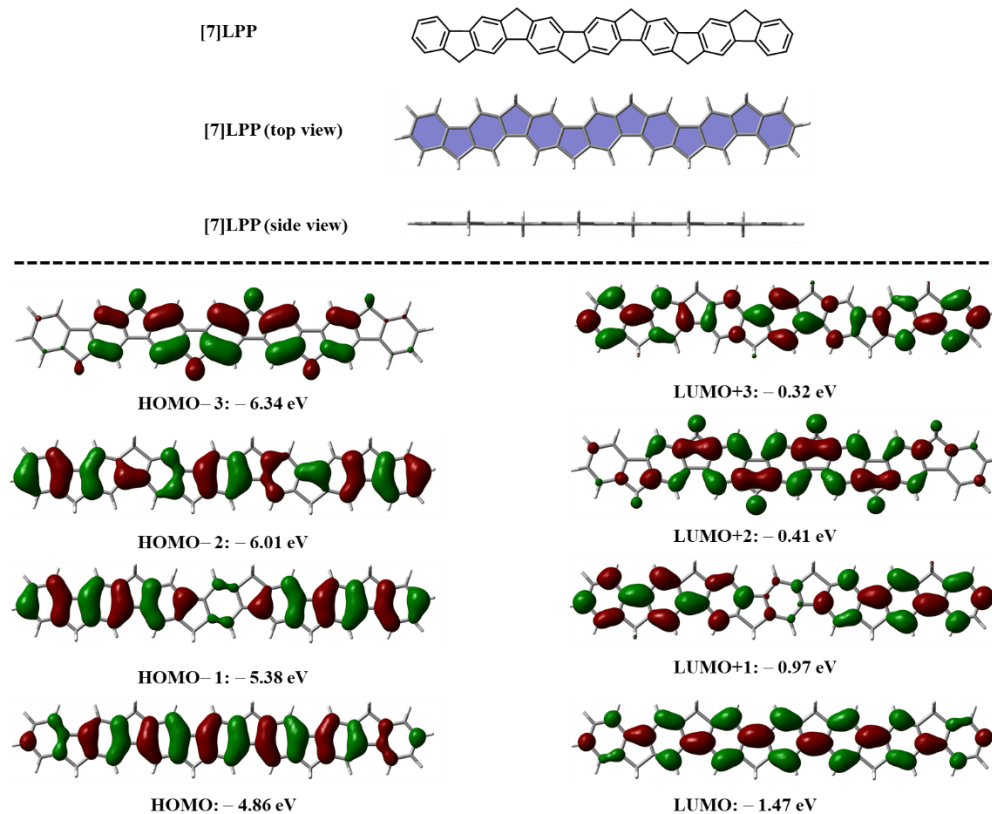


Figure S4. The frontier orbital energies of [7]LPP calculated by B3LYP/6-31G(d).

4. Computational study

The Gaussian 16 program⁸ running on the NEC LX system was used for optimization (B3LYP/6-31G(d)).⁹ Structures were optimized without any symmetry assumptions. Zero-point energy, enthalpy, and Gibbs free energy at 298.15 K and 1 atm were estimated from the gas-phase studies. Harmonic vibration frequency calculation at the same level was performed to verify all stationary points as local minima (with no imaginary frequency) or transition states (with one imaginary frequency). IRC calculations were also performed to check transition states. Visualization of the results was performed by the use of GaussView 5.0.9 software.

4.1 HOMO and LUMO energies of [n]CPP, methylene-bridged [n]CPP, and [n]LPP

Table S4. The frontier orbital energies of [n]CPP, methylene-bridged [n]CPP and [n]LPP series calculated by B3LYP/6-31G(d) level of theory with Gaussian 16 program (unit: eV).

	[n]CPP		[n]LPP		CH ₂ -bridged [n]CPP	
<i>n</i>	HOMO	LUMO	HOMO	LUMO	HOMO	LUMO
6	−4.92	−1.78	−4.92	−1.42	−4.40	−1.74
8	−5.10	−1.70	−4.82	−1.50	−4.48	−1.71
10	−5.20	−1.66	−4.77	−1.55	−4.53	−1.69
12	−5.25	−1.64	−4.73	−1.58	−4.56	−1.68
14	−5.29	−1.63	−4.71	−1.60	−4.58	−1.67
16	−5.31	−1.62	−4.70	−1.61	−4.60	−1.67
18	−5.33	−1.62	−4.69	−1.62	−4.60	−1.66
20	−5.34	−1.61	−4.68	−1.62	−4.61	−1.66

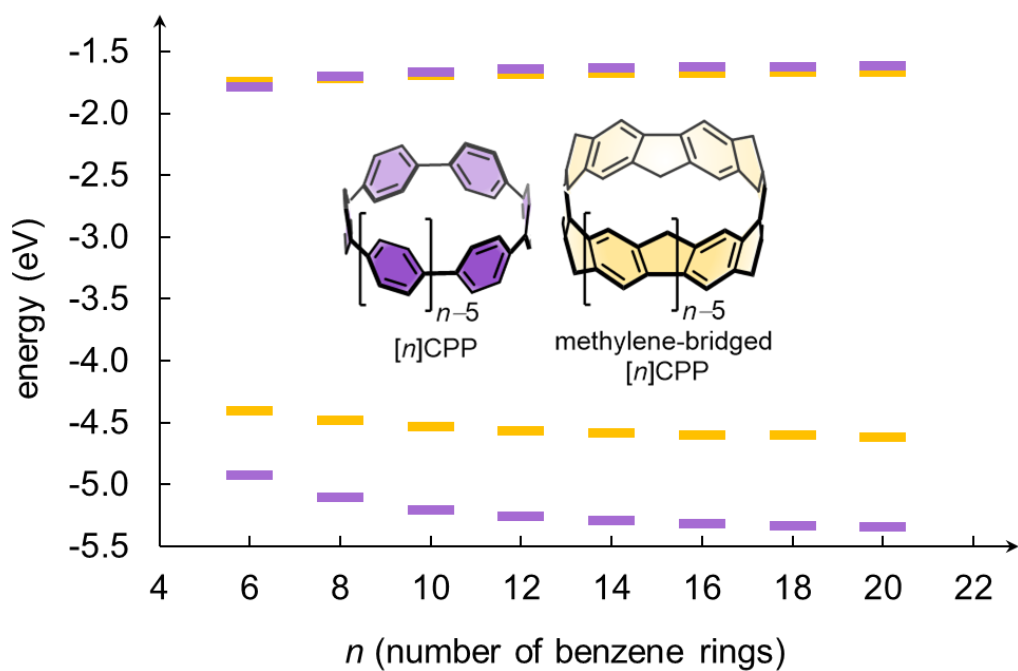


Figure S5. HOMO and LUMO energies of $[n]$ CPP (purple) and methylene-bridged $[n]$ CPP (orange) calculated at the B3LYP/6-31G(d) level of theory.

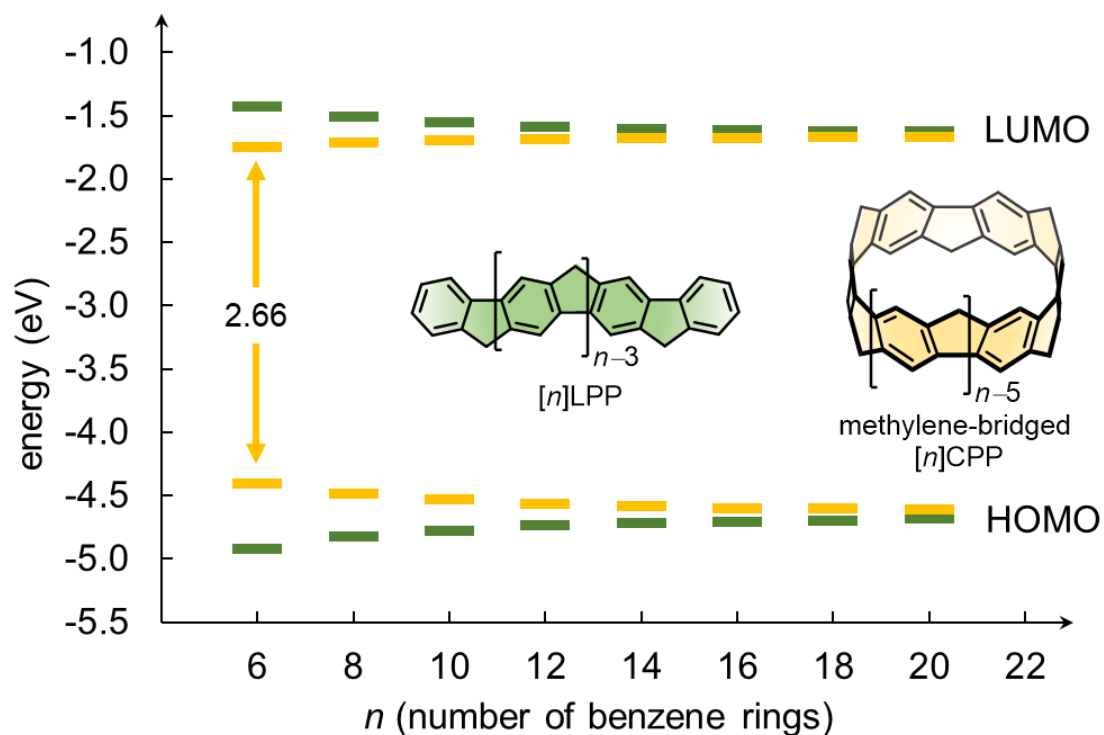
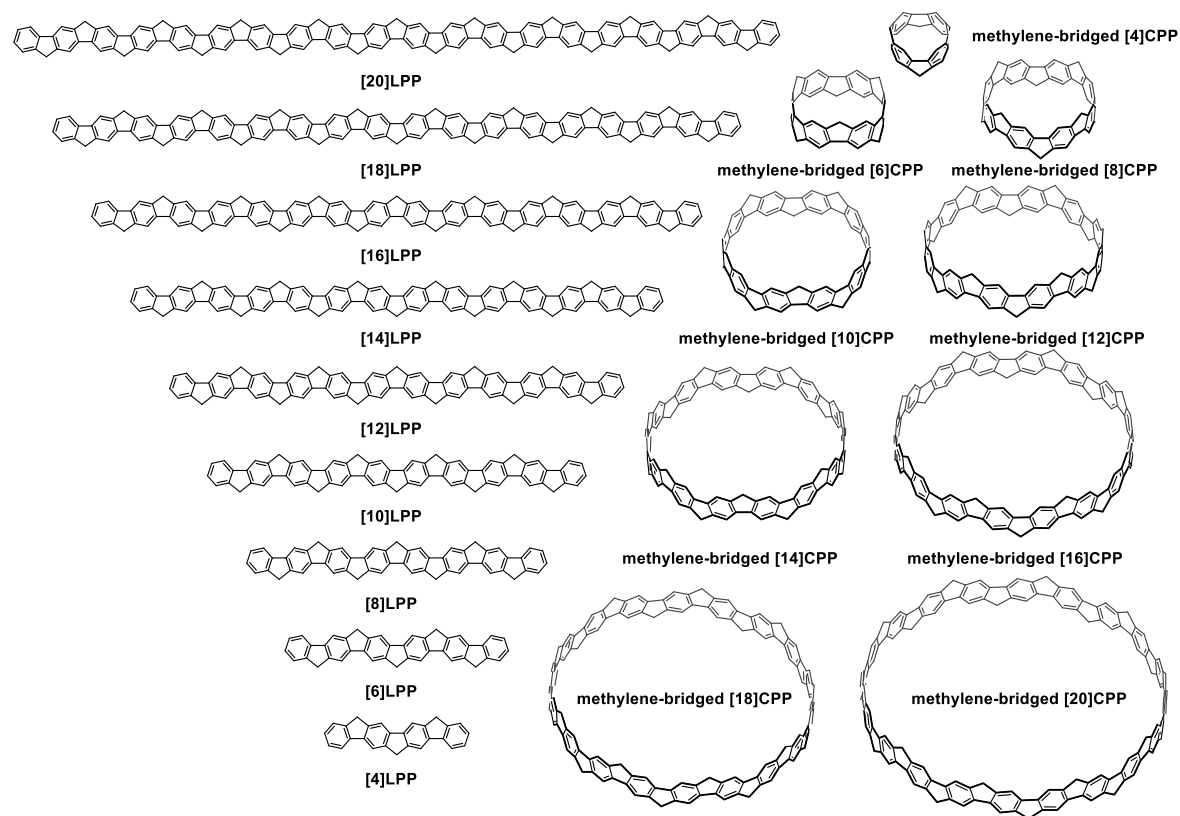


Figure S6. HOMO and LUMO energies of $[n]$ LPP (green) and methylene-bridged $[n]$ CPP (orange) calculated at the B3LYP/6-31G(d) level of theory.

4.2 Optimized structures and frontier molecular orbitals

Scheme S2. The optimized structures and frontier orbital energies of $[n]$ CPP, methylene-bridged $[n]$ CPP and $[n]$ LPP series calculated by B3LYP/6-31G(d).



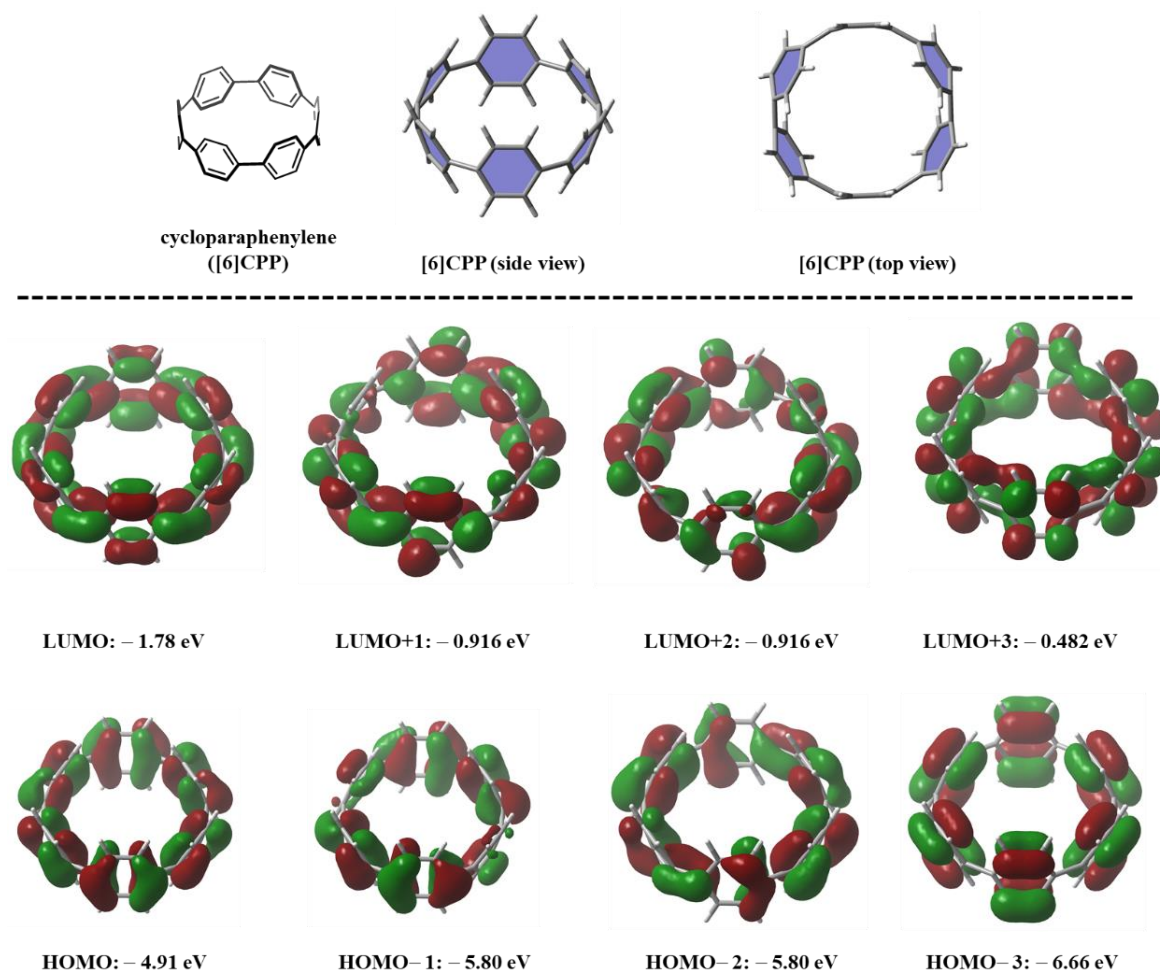


Figure S7. The optimized structures and frontier orbital energies of [6]CPP calculated by B3LYP/6-31G(d) level of theory.

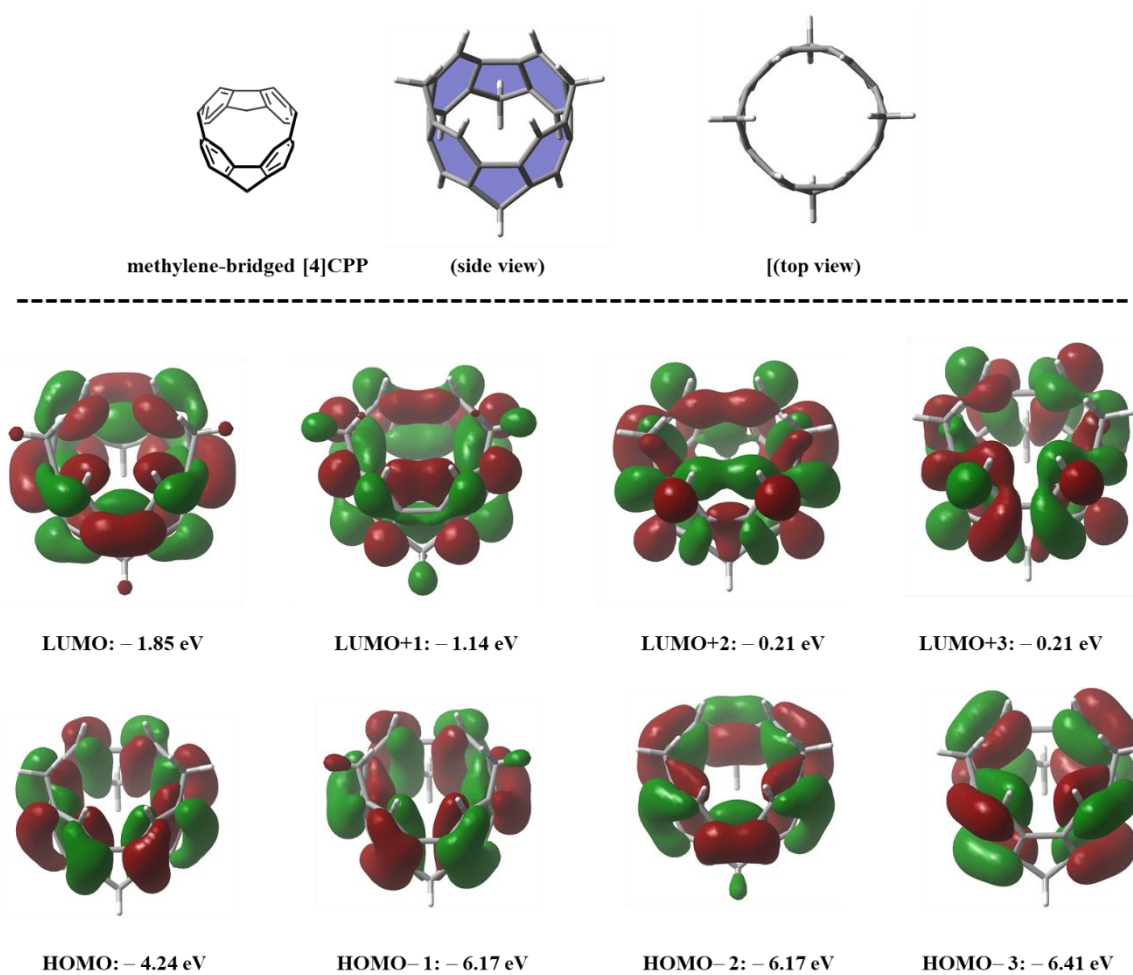


Figure S8. The optimized structures and frontier orbital energies of methylene-bridged [4]CPP calculated by B3LYP/6-31G(d) level of theory.

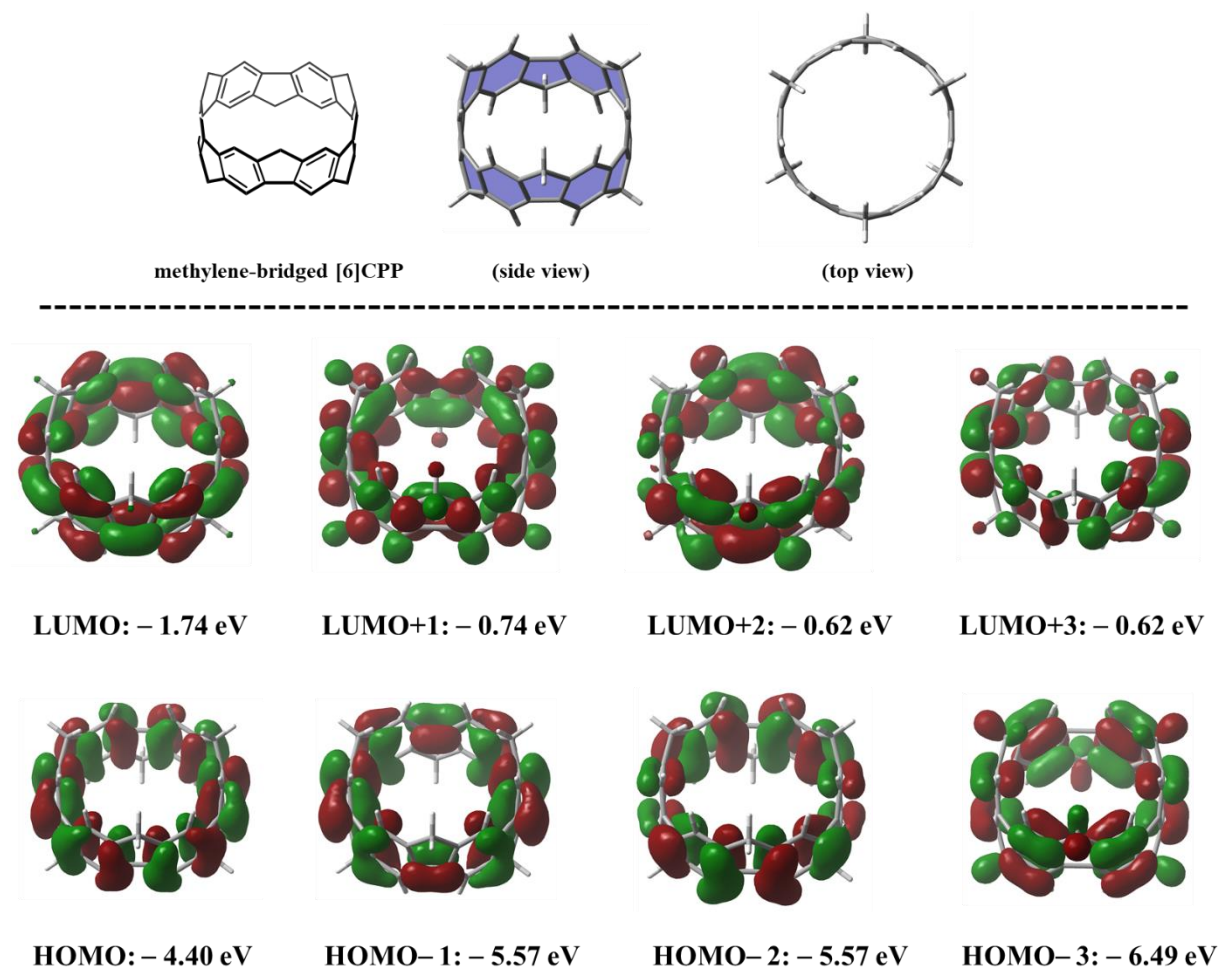


Figure S9. The optimized structures and frontier orbital energies of methylene-bridged [6]CPP calculated by B3LYP/6-31G(d) level of theory.

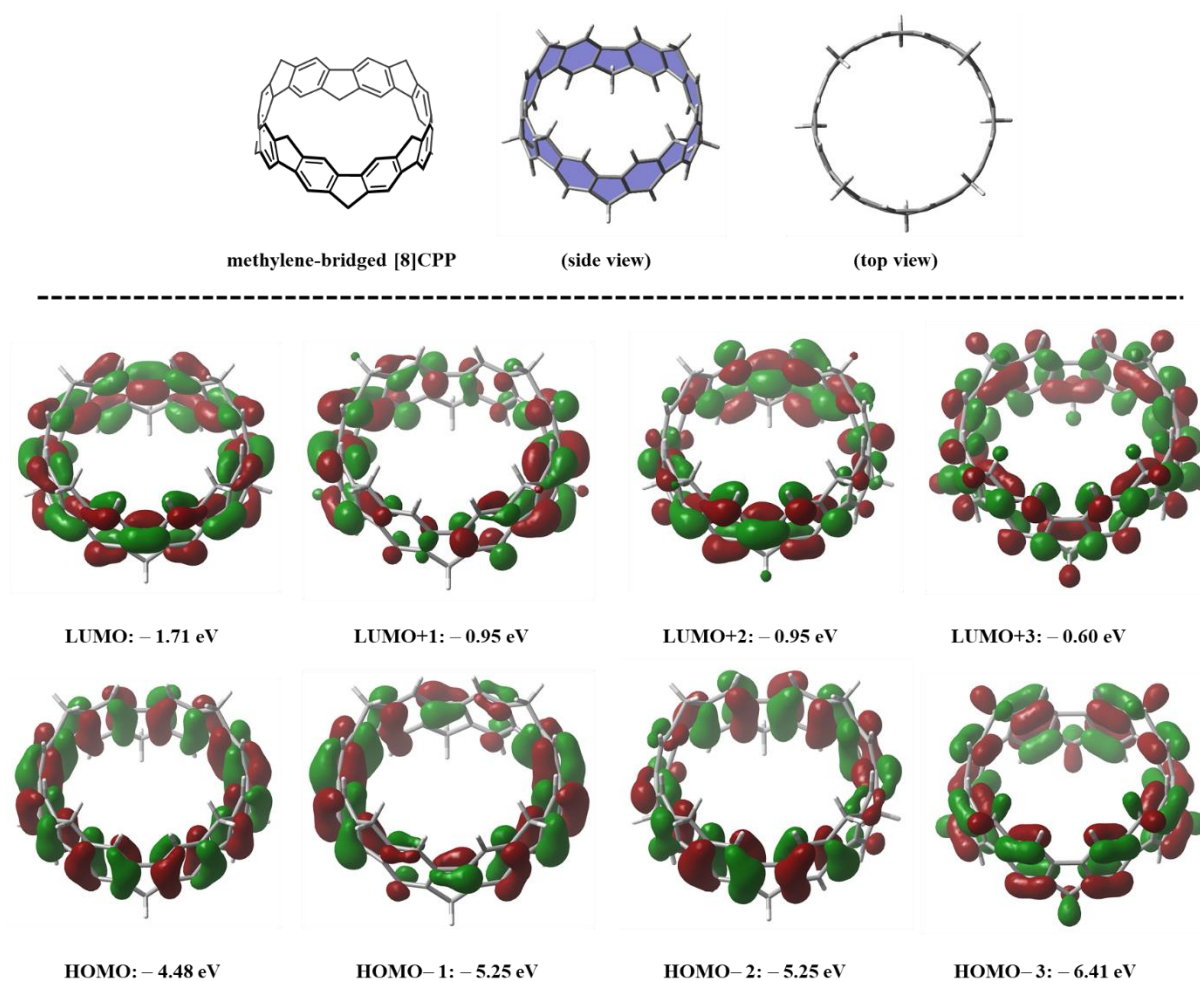


Figure S10. The optimized structures and frontier orbital energies of methylene-bridged [8]CPP calculated by B3LYP/6-31G(d) level of theory.

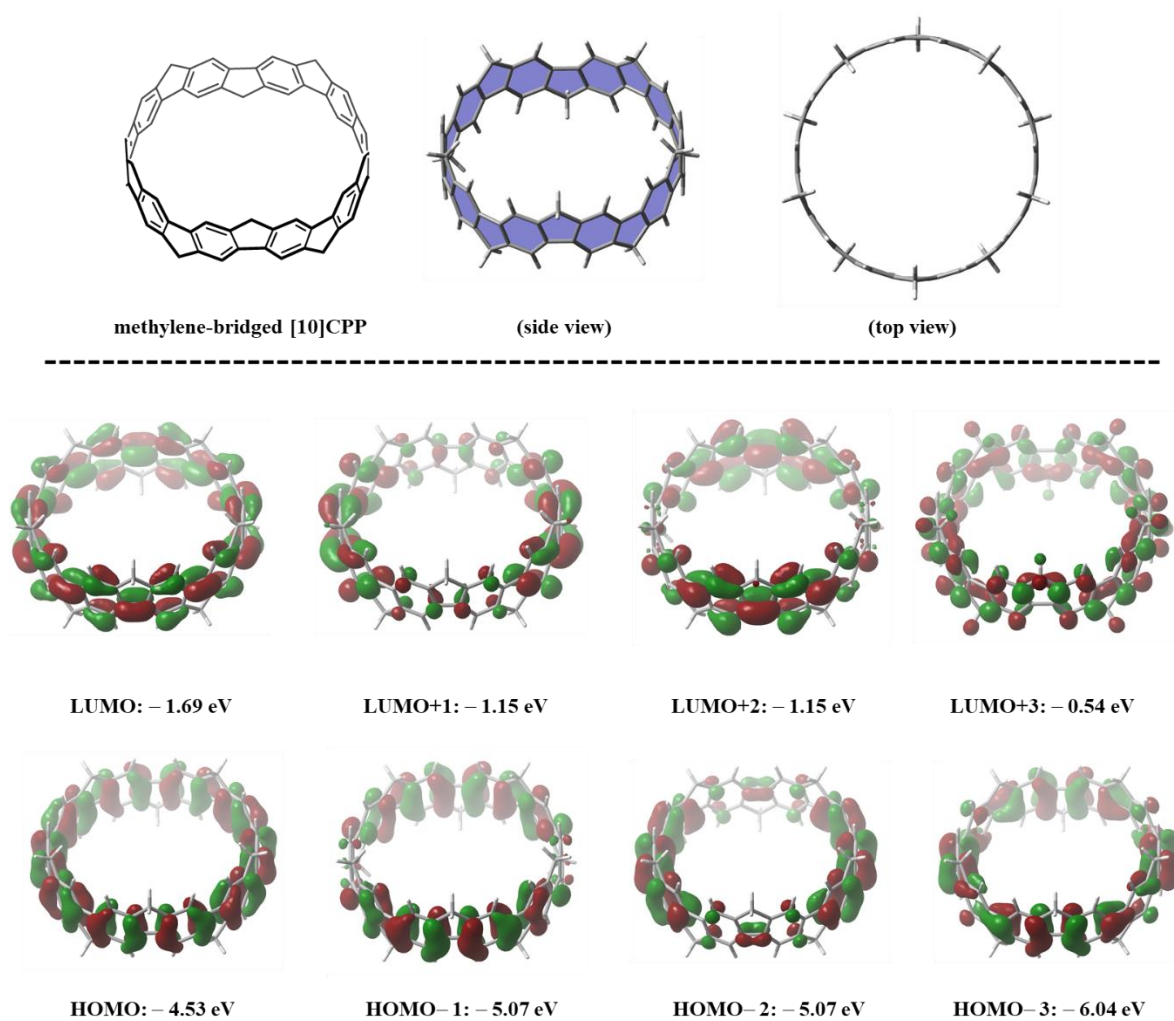


Figure S11. The optimized structures and frontier orbital energies of methylene-bridged [10]CPP calculated by B3LYP/6-31G(d) level of theory.

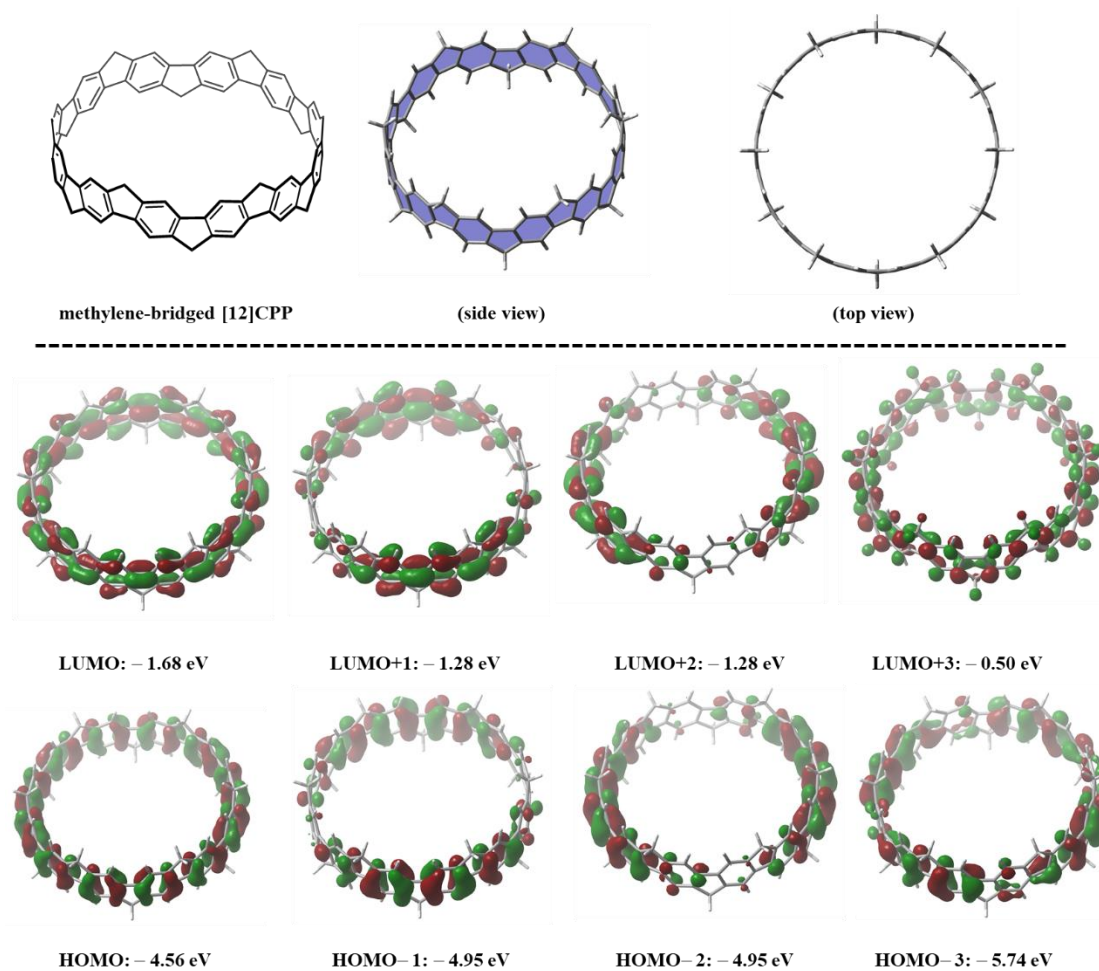


Figure S12. The optimized structures and frontier orbital energies of methylene-bridged [12]CPP calculated by B3LYP/6-31G(d) level of theory.

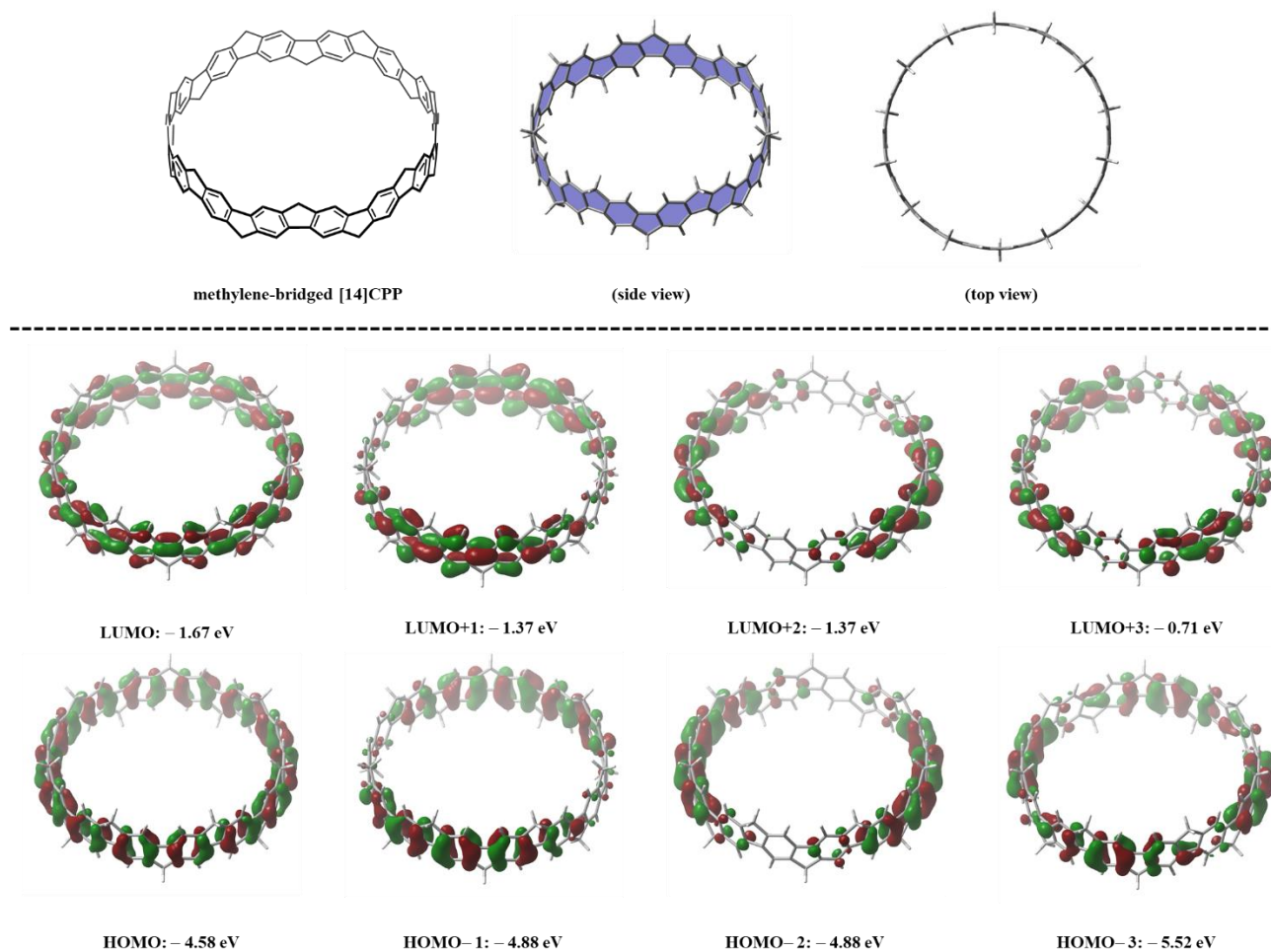


Figure S13. The optimized structures and frontier orbital energies of methylene-bridged [14]CPP calculated by B3LYP/6-31G(d) level of theory.

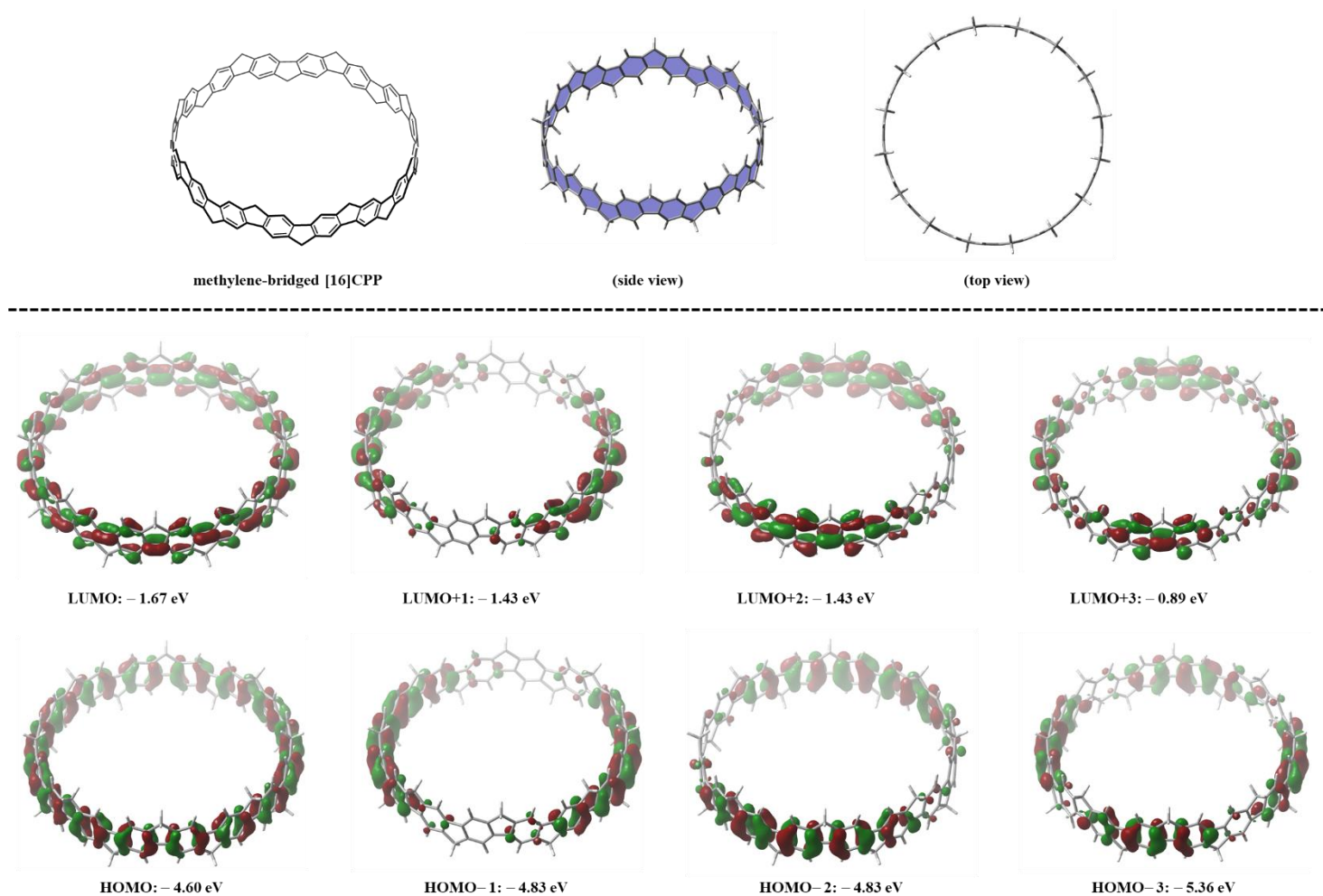


Figure S14. The optimized structures and frontier orbital energies of methylene-bridged [16]CPP calculated by B3LYP/6-31G(d) level of theory.

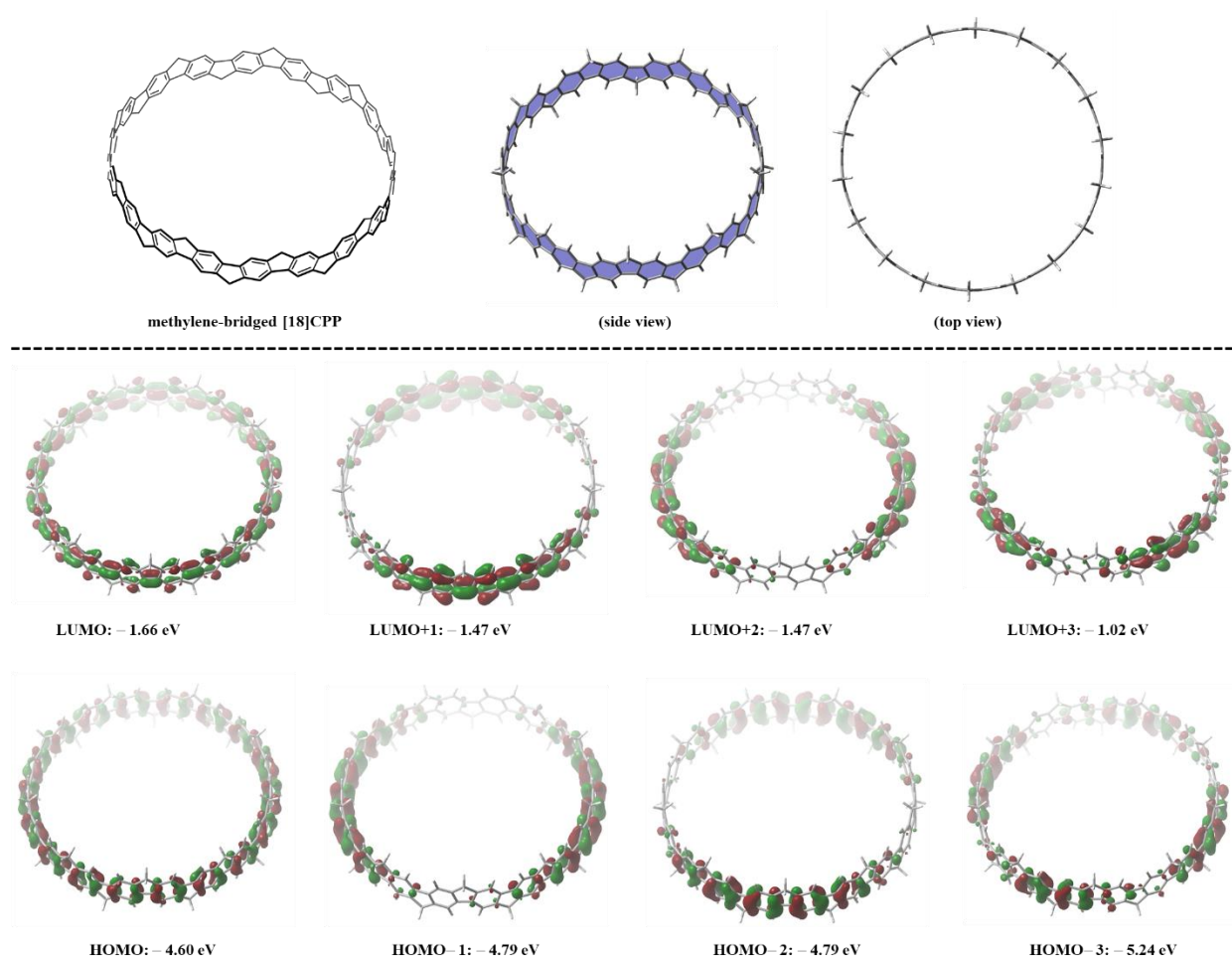


Figure S15. The optimized structures and frontier orbital energies of methylene-bridged [18]CPP calculated by B3LYP/6-31G(d) level of theory.

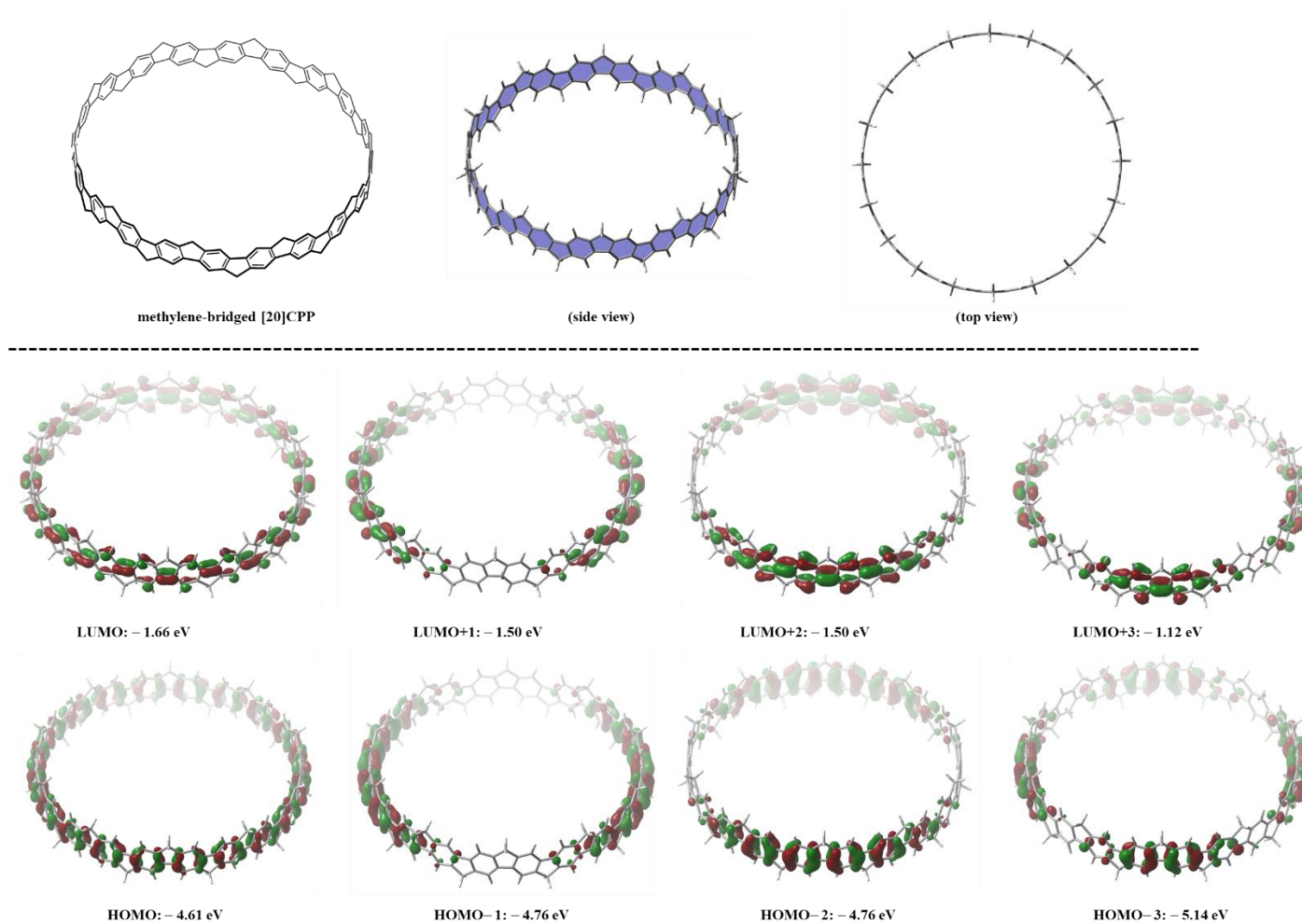


Figure S16. The optimized structures and frontier orbital energies of methylene-bridged [20]CPP calculated by B3LYP/6-31G(d) level of theory.

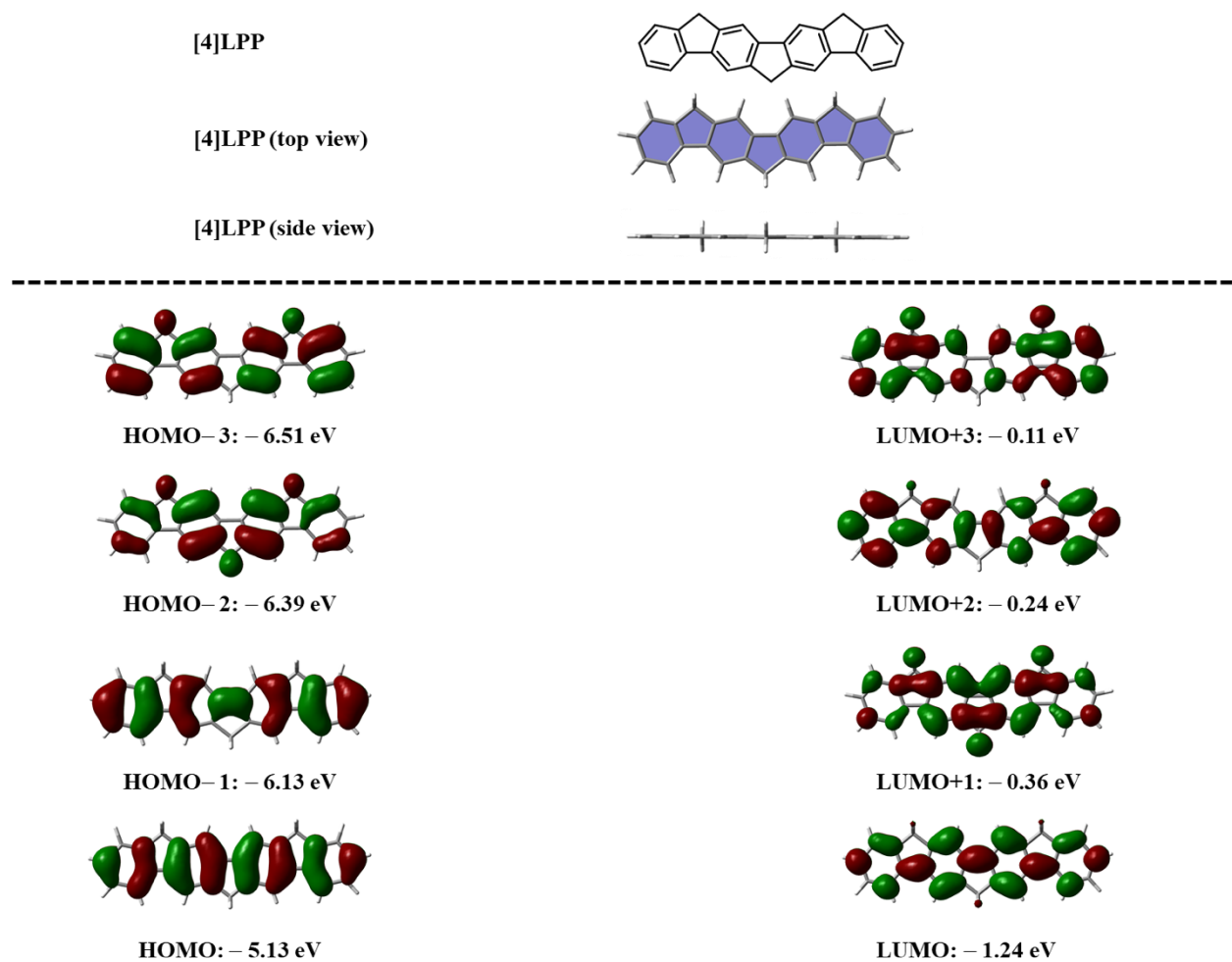


Figure S17. The optimized structures and frontier orbital energies of [4]LPP calculated by B3LYP/6-31G(d) level of theory.

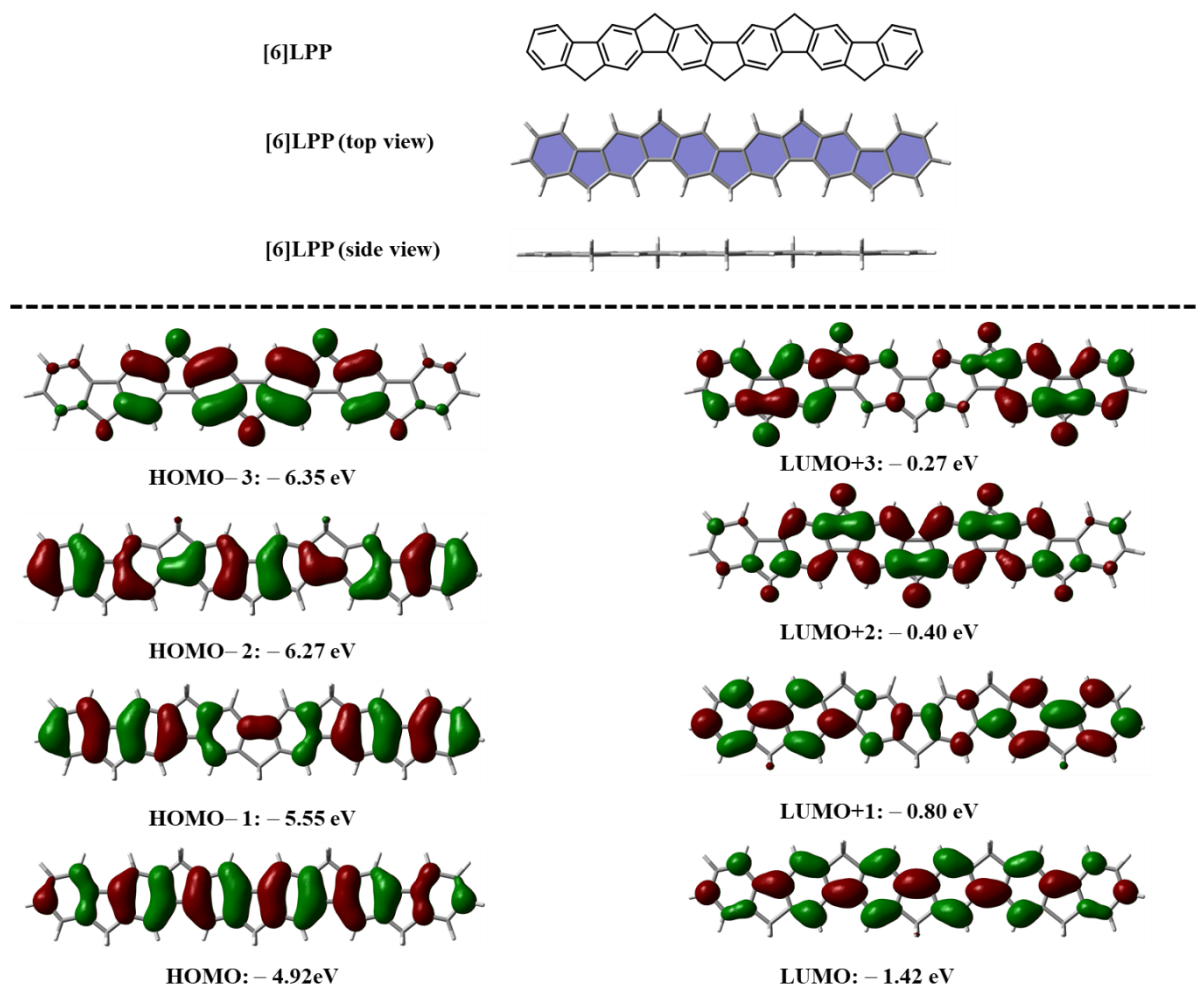


Figure S18. The optimized structures and frontier orbital energies of [6]LPP calculated by B3LYP/6-31G(d) level of theory.

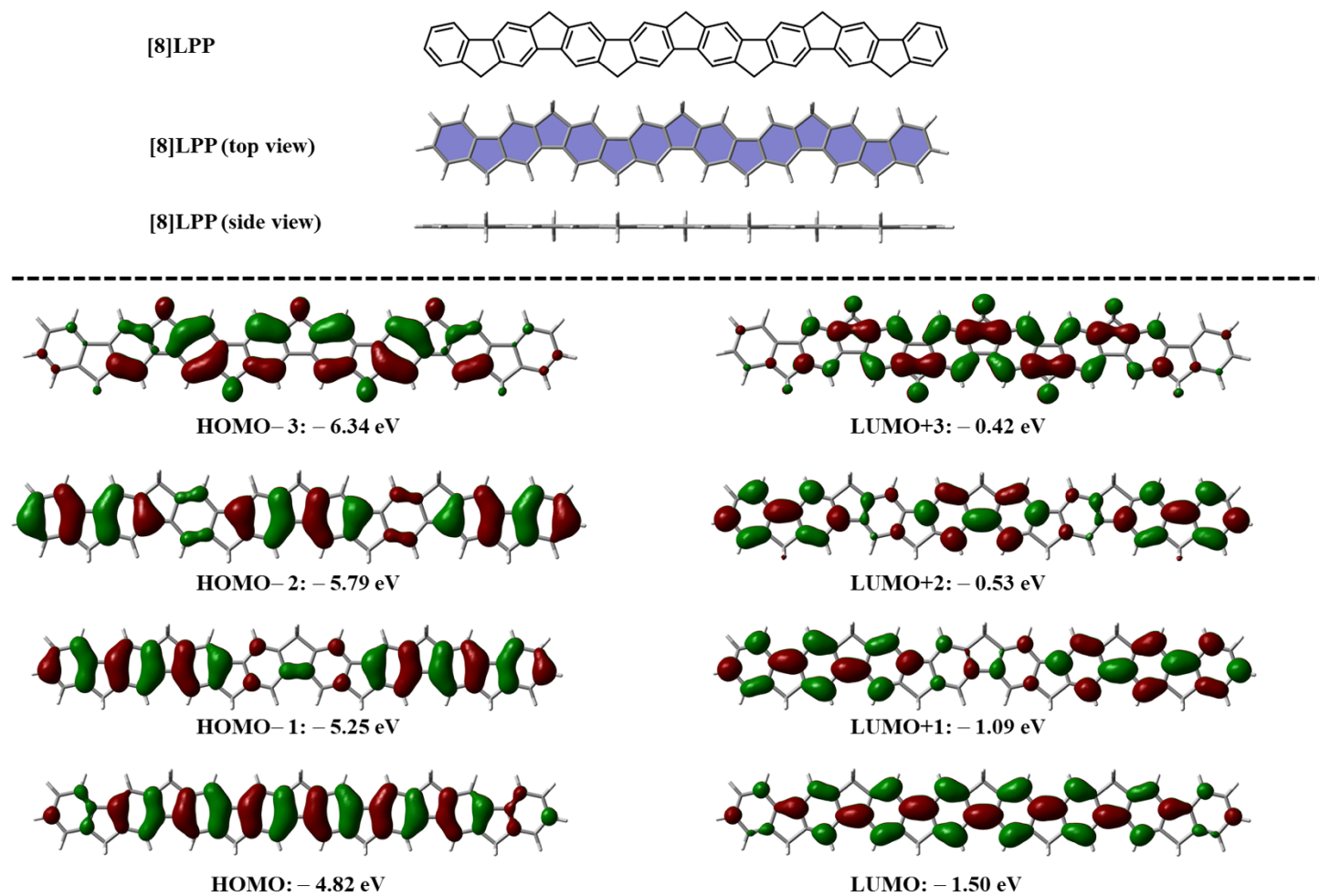


Figure S19. The optimized structures and frontier orbital energies of [8]LPP calculated by B3LYP/6-31G(d) level of theory.

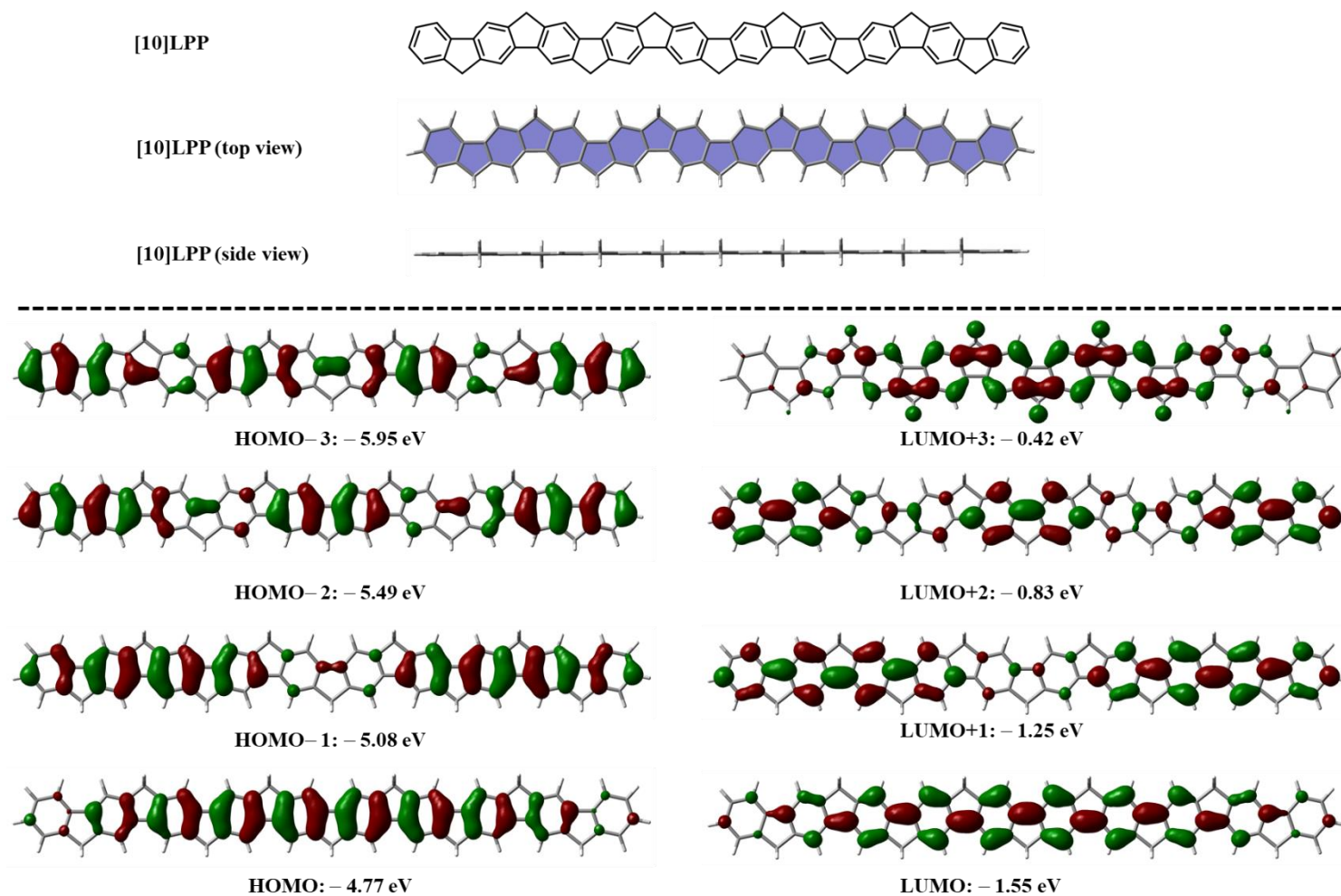


Figure S20. The optimized structures and frontier orbital energies of [10]LPP calculated by B3LYP/6-31G(d) level of theory.

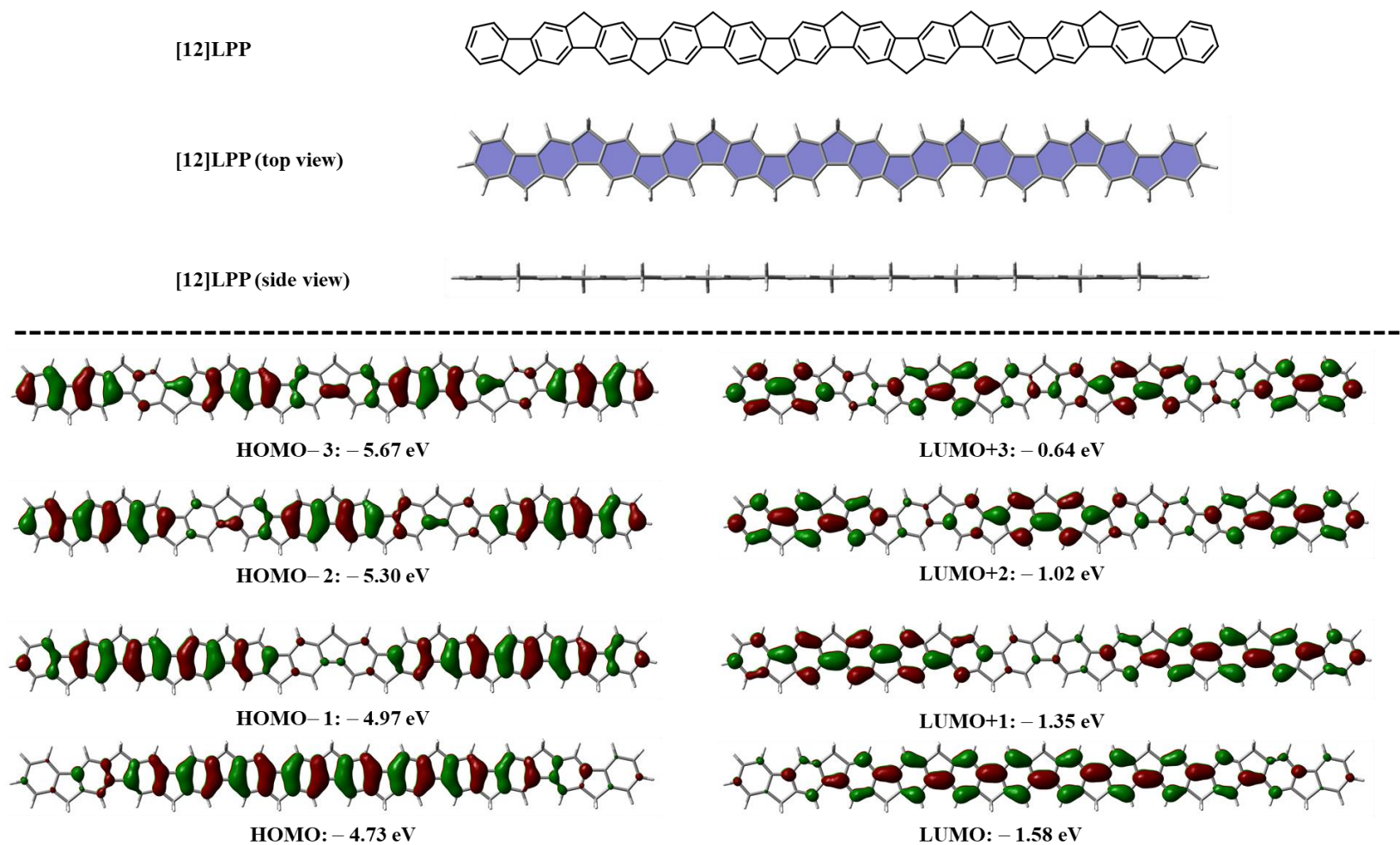


Figure S21. The optimized structures and frontier orbital energies of [12]LPP calculated by B3LYP/6-31G(d) level of theory.

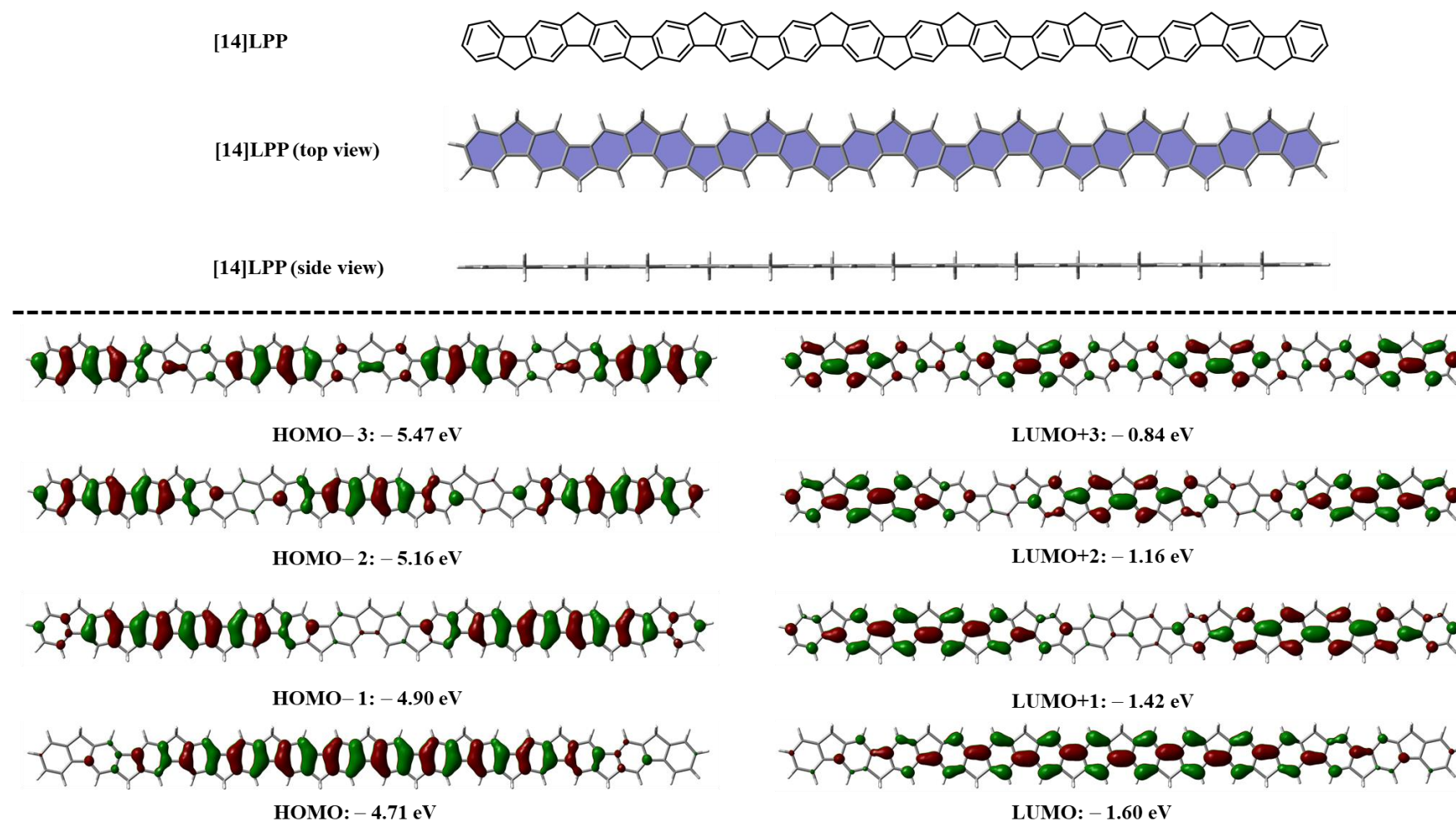


Figure S22. The optimized structures and frontier orbital energies of [14]LPP calculated by B3LYP/6-31G(d) level of theory.

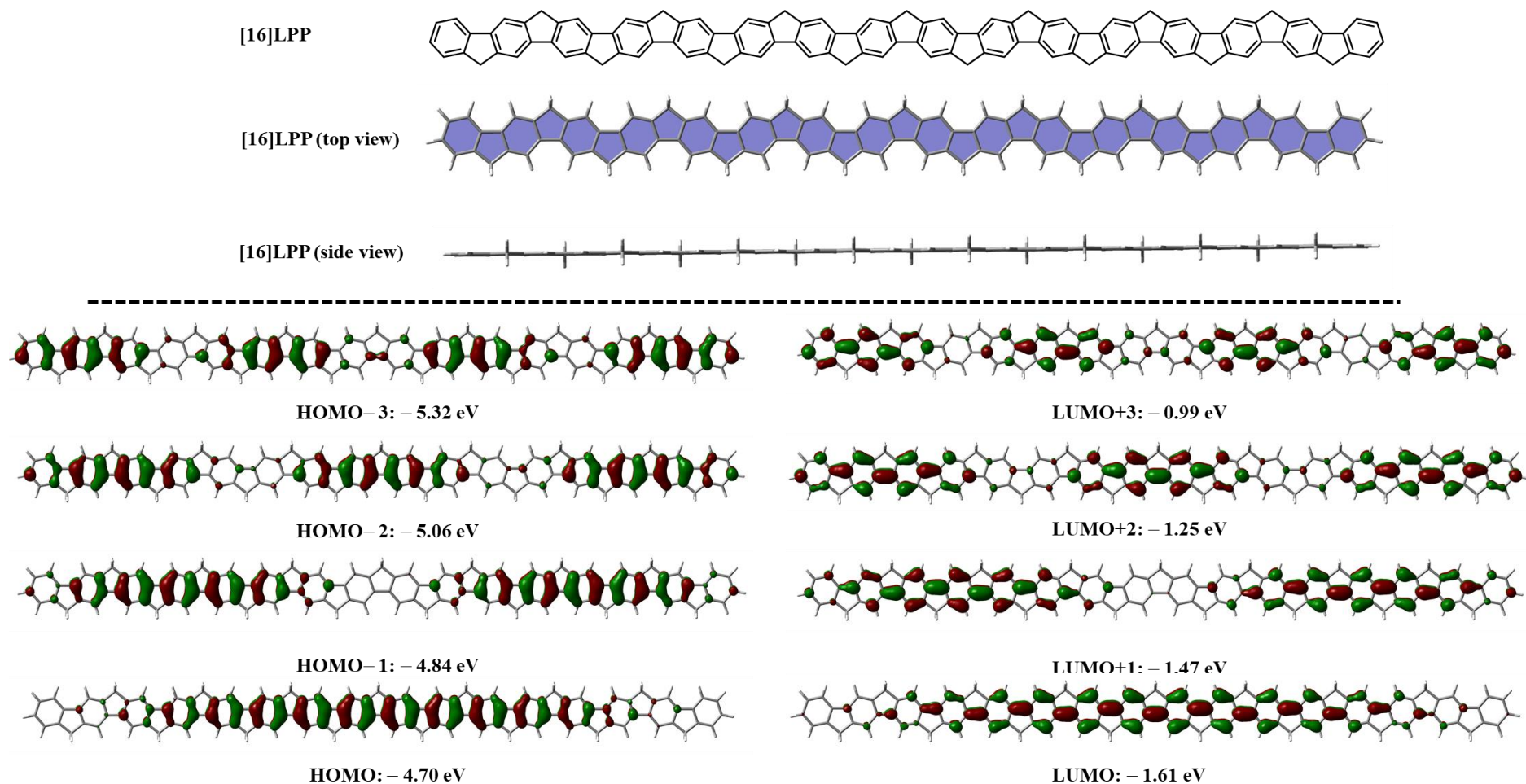


Figure S23. The optimized structures and frontier orbital energies of [16]LPP calculated by B3LYP/6-31G(d) level of theory.

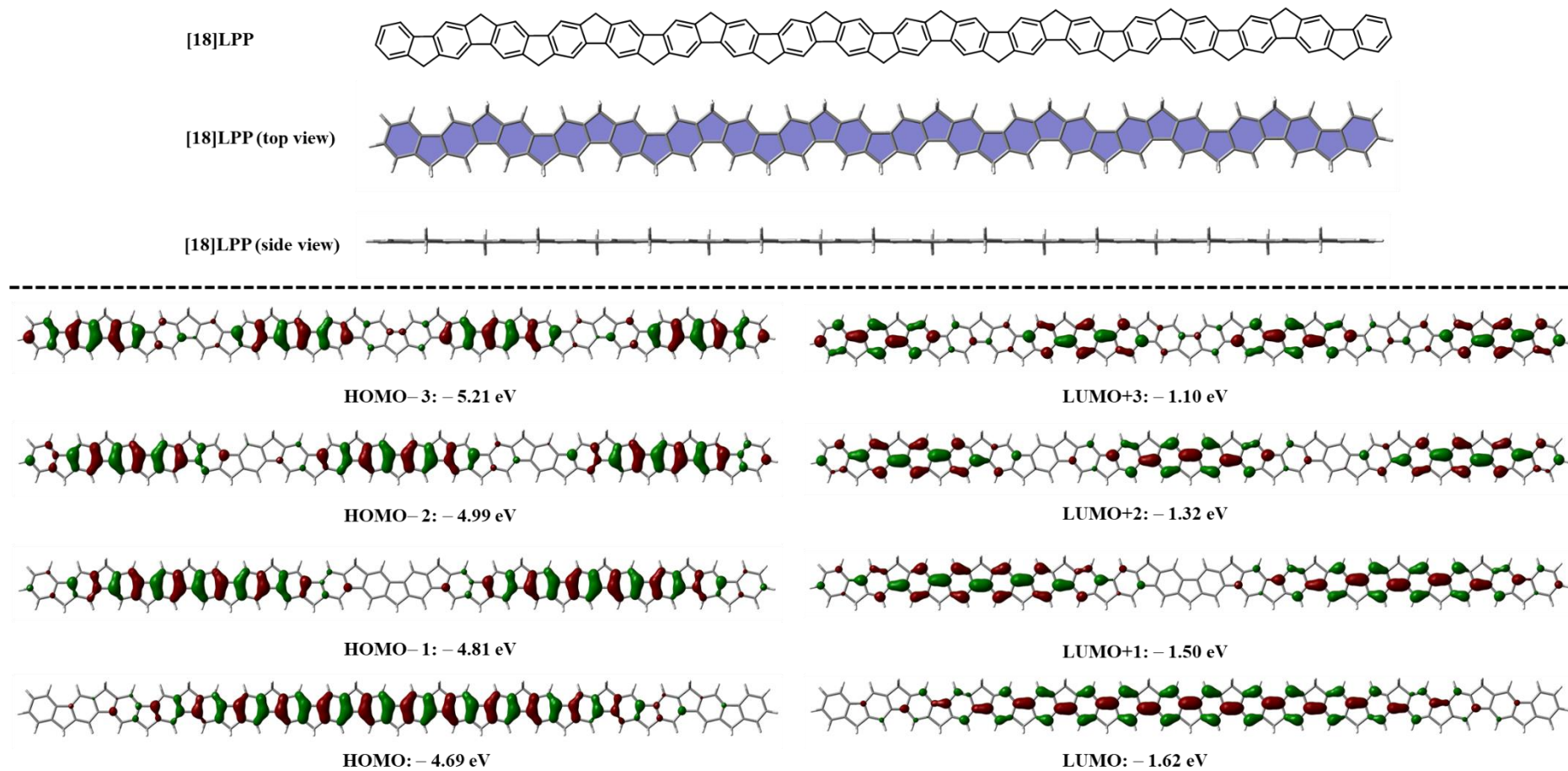


Figure S24. The optimized structures and frontier orbital energies of [18]LPP calculated by B3LYP/6-31G(d) level of theory.

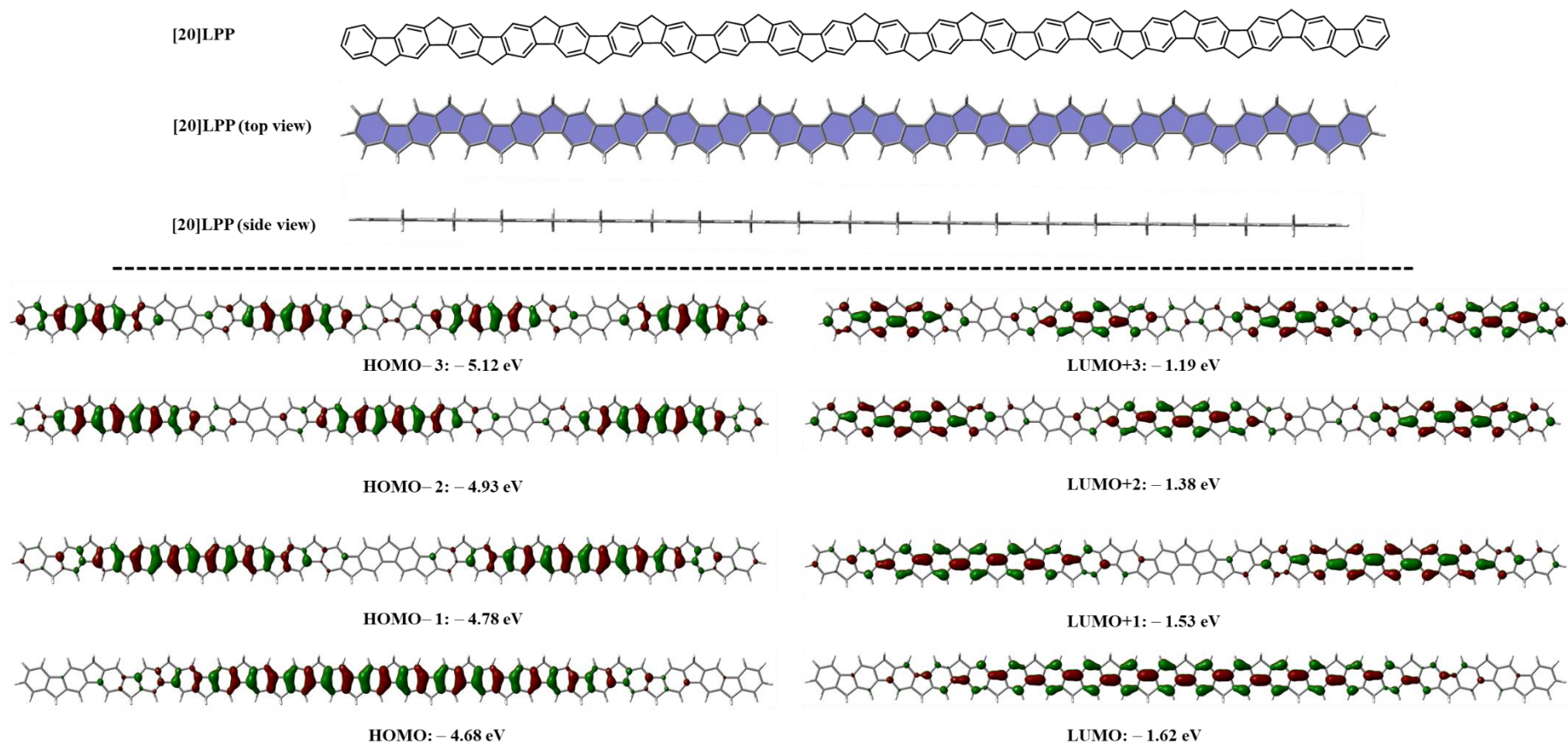
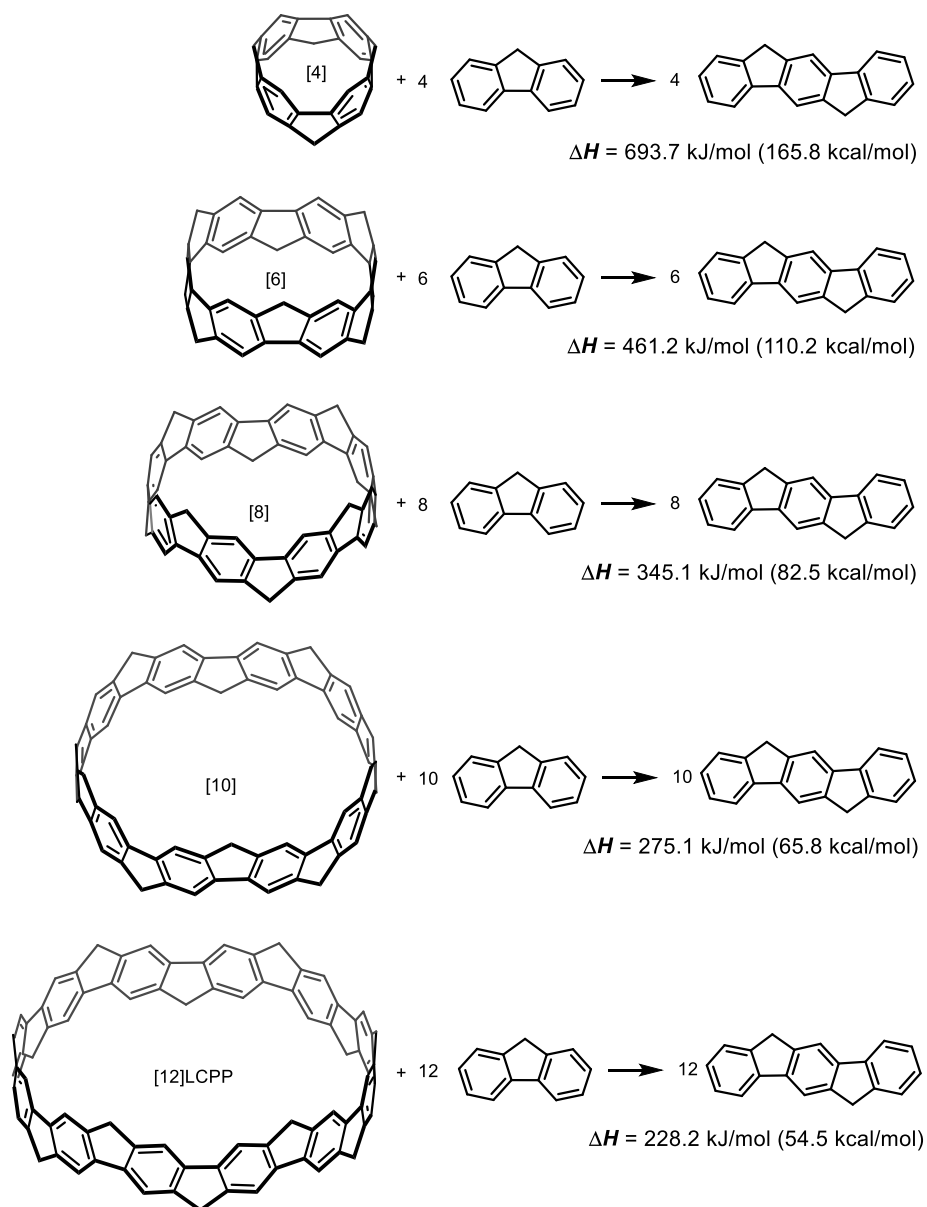


Figure S25. The optimized structures and frontier orbital energies of [20]LPP calculated by B3LYP/6-31G(d) level of theory..

4.3 The calculation of strain energy¹⁰

Scheme S3. Homodesmotic reactions for the calculation of strain energies for methylene-bridged $[n]$ CPP calculated by B3LYP/6-31G(d) level of theory respectively.



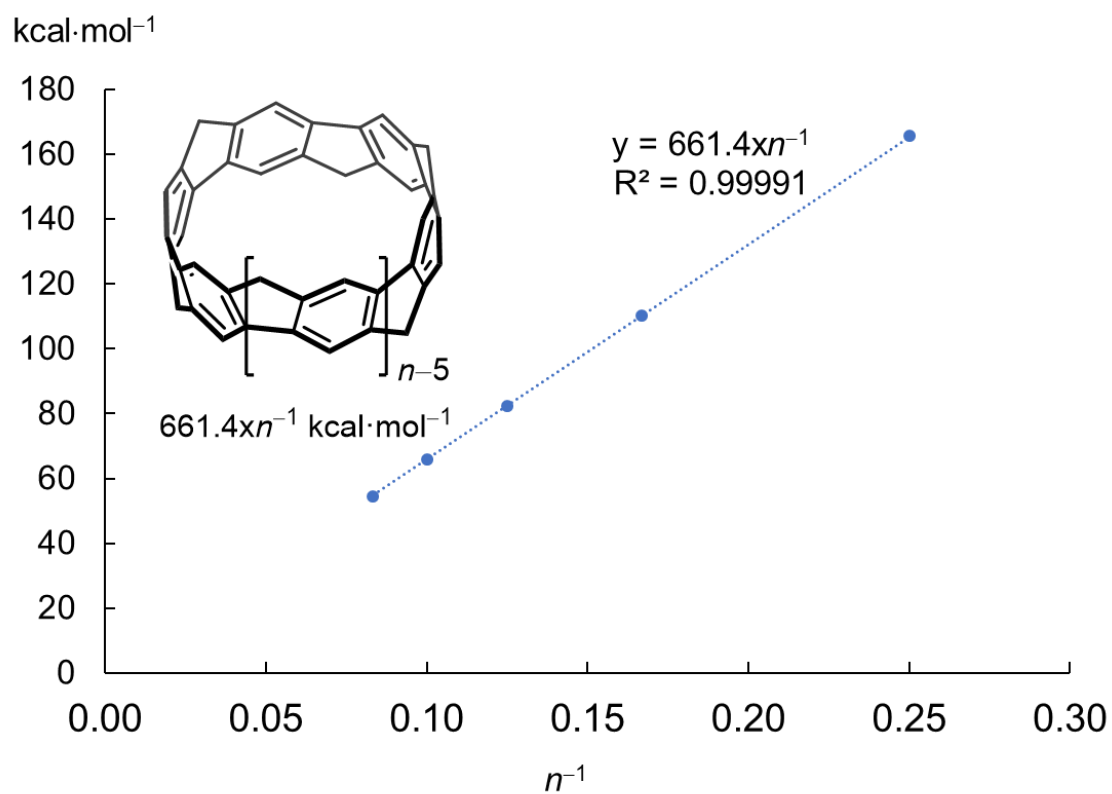
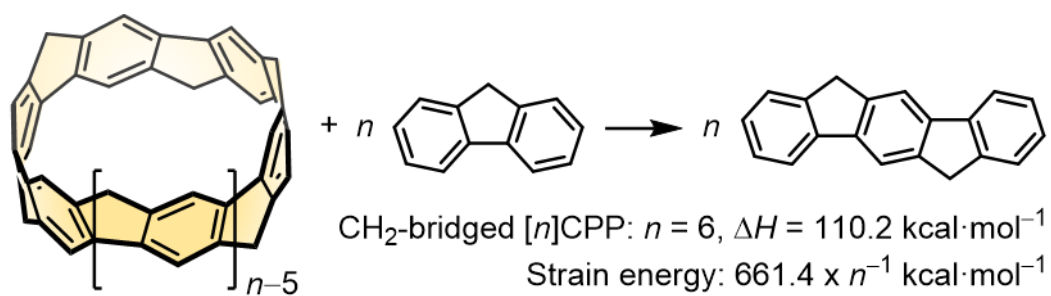
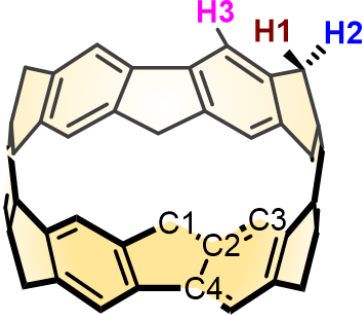


Figure S26. Plot of the strain energy with linear regression line.

4.4 Simulated NMR chemical shifts (ppm)

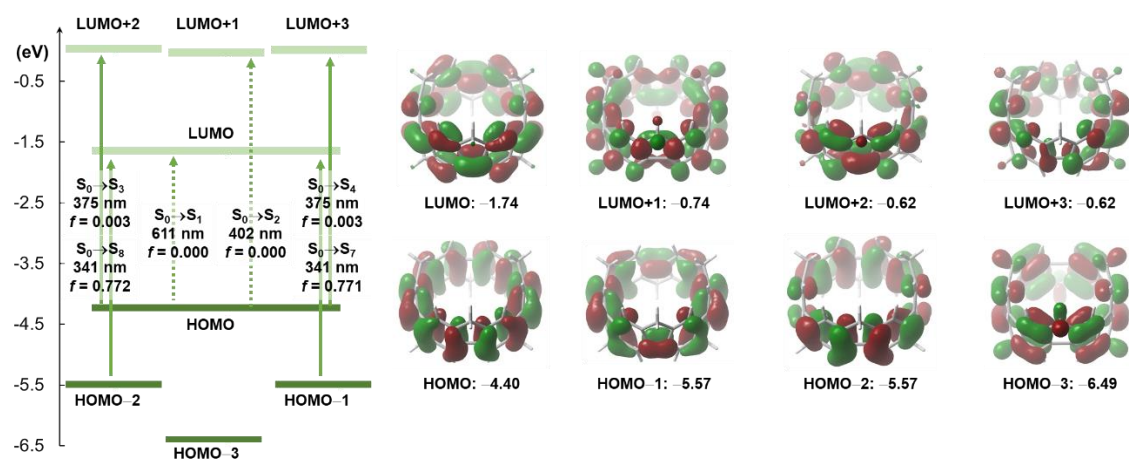
Table S5. Simulated NMR chemical shifts (ppm) calculated by B3LYP/6-311+G(2d,p) level of theory. Geometry optimization of **4** was calculated by B3LYP/6-31G(d).

		simulated	observed in CD ₂ Cl ₂
	H3	8.31	7.86
	H2	4.47 (outer)	4.29
	H1	4.32 (inner)	4.09
	C2	156.1	148.0
	C4	142.5	137.1
	C3	125.3	121.8
	C1	45.3	40.9

4.5 TD-DFT vertical one-electron excitations

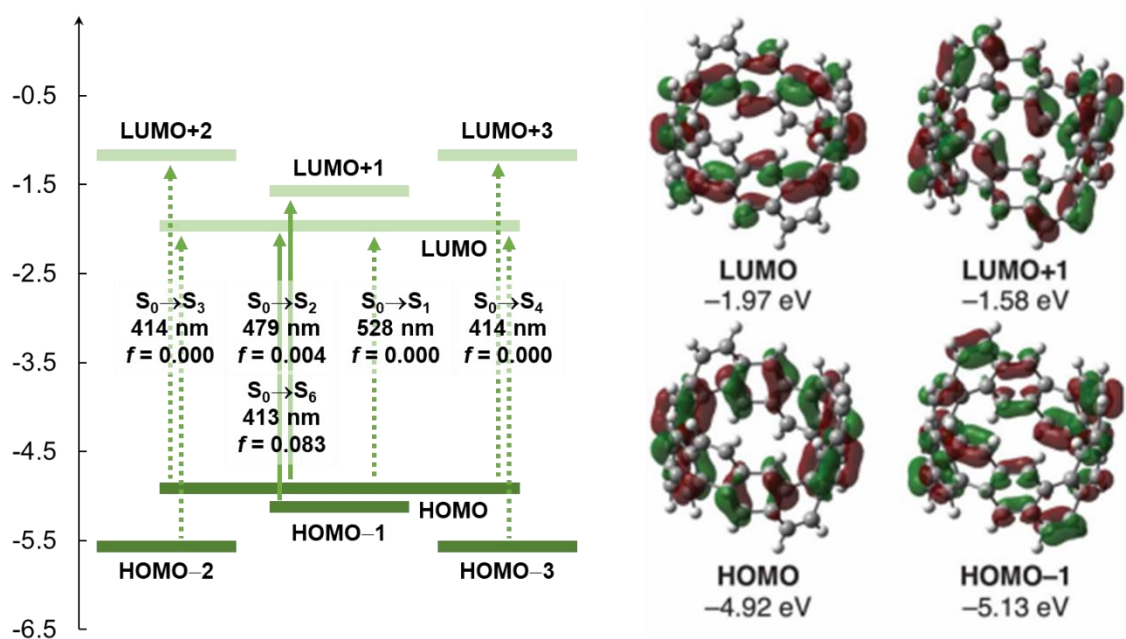
Table S6. Major electronic transitions for **4** by TD-DFT method using B3LYP/6-31G(d).

	energy (eV)	Excitation [nm]	Oscillator strength (f)	Description
S1	2.0296	610.89	0.0000	H→L (0.70517)
S2	3.0826	402.21	0.0000	H→L+1 (0.69621)
S3	3.3037	375.29	0.0027	H-2→L (-0.45228); H→L+2 (0.51103); H→L+3 (-0.15142)
S4	3.3037	375.29	0.0027	H-1→L (0.45235); H→L+3 (0.51093); H→L+2 (0.15140)
S5	3.4303	361.44	0.0003	H→L+4 (0.67860)
S6	3.4303	361.43	0.0003	H→L+5 (0.67864)
S7	3.6309	341.47	0.7714	H-1→L (0.52617); H→L+3 (-0.44484)
S8	3.6309	341.47	0.7715	H-2→L (0.52630); H→L+2 (0.44472)
S11	4.1792	296.67	0.0252	H-3→L (0.63741); H→L (0.24758)
S19	4.4372	279.42	0.0439	H-6→L (0.60029); H-1→L+1 (-0.32050)



Major electronic transitions for [6,6]CNB by TD-DFT method using B3LYP/6-31G(d).

	energy (eV)	Excitation [nm]	Oscillator strength (f)	Description
S1	2.3475	528.16	0.0000	H→L (0.70267)
S2	2.5870	479.25	0.0038	H-1→L (0.59483); H→L+1 (0.36630)
S3	2.9975	413.62	0.0000	H-2→L (0.57315); H→L+2 (0.37325)
S4	2.9980	413.56	0.0000	H-3→L (0.57328); H→L+3 (0.37325)
S5	3.0017	413.04	0.0000	H-1→L+1 (0.69572)
S6	3.0046	412.64	0.0828	H-1→L (0.37159); H→L+1 (0.59477)
S18	3.8386	323.00	0.7244	H-4→L (0.39610); H-2→L+1 (-0.30692); H→L+4 (0.29796);



4.6 Uncorrected and thermal-corrected energies of stationary points

Table S7. Uncorrected and thermal-corrected (298 K) energies of stationary points (Hartree) ([*n*]CPP, methylene-bridged [*n*]CPP and [*n*]LPP, B3LYP/6-31G(d)).

Compound	<i>E</i> + <i>ZPE</i>	<i>E</i>	<i>H</i>	<i>G</i>
[4]CPP	−923.676125	−923.660701	−923.659756	−923.716499
[6]CPP	−1385.705155	−1385.679890	−1385.678946	−1385.757072
[8]CPP	−1847.696459	−1847.661820	−1847.660876	−1847.759410
[10]CPP	−2309.672941	−2309.628859	−2309.627915	−2309.748712
[12]CPP	−2771.641932	−2771.588385	−2771.587441	−2771.729449
[14]CPP	−3233.606496	−3233.543473	−3233.542529	−3233.709158
[16]CPP	−3695.568316	−3695.495816	−3695.494872	−3695.682502
[18]CPP	−4157.528327	−4157.446342	−4157.445397	−4157.656202
[20]CPP	−4619.487021	−4619.395550	−4619.394606	−4619.628631
CH ₂ -[4]CPP	−1076.084241	−1076.067693	−1076.066748	−1076.125470
CH ₂ -[6]CPP	−1614.347805	−1614.321728	−1614.320783	−1614.399318
CH ₂ -[8]CPP	−2152.567254	−2152.531404	−2152.530460	−2152.629646
CH ₂ -[10]CPP	−2690.769225	−2690.723542	−2690.722598	−2690.840623
CH ₂ -[12]CPP	−3228.962423	−3228.906884	−3228.905939	−3229.047419
CH ₂ -[14]CPP	−3767.150612	−3767.085217	−3767.084273	−3767.246486
CH ₂ -[16]CPP	−4305.335683	−4305.260414	−4305.259470	−4305.443962
CH ₂ -[18]CPP	−4843.518610	−4843.433489	−4843.432545	−4843.638616
CH ₂ -[20]CPP	−5381.700082	−5381.605105	−5381.604160	−5381.831886
[4]LPP	−1039.410002	−1039.391385	−1039.390441	−1039.456694
[6]LPP	−1577.585436	−1577.557009	−1577.556064	−1577.644634
[8]LPP	−2115.760889	−2115.722635	−2115.721691	−2115.832590
[10]LPP	−2653.936345	−2653.888256	−2653.887312	−2654.020537
[12]LPP	−3192.111806	−3192.053883	−3192.052938	−3192.208486
[14]LPP	−3730.287268	−3730.219509	−3730.218565	−3730.395803
[16]LPP	−4268.462732	−4268.385134	−4268.384190	−4268.584395
[18]LPP	−4806.638196	−4806.550758	−4806.549814	−4806.772359
[20]LPP	−5344.813660	−5344.716384	−5344.715440	−5344.960322

[a] *E*: electronic energy; *ZPE*: zero-point energy; *H* ($= E + ZPE + E_{\text{vib}} + E_{\text{rot}} + E_{\text{trans}} + RT$): sum of electronic and thermal enthalpies; *G* ($= H - TS$): sum of electronic and thermal free energies.

4.7 Cartesian coordinates of optimized structures

Cartesian coordinates of optimized structures calculated by B3LYP/6-31G(d) level of theory ($[n]$ CPP, methylene-bridged $[n]$ CPP, and $[n]$ LPP). See attached file (Cartesian_coordinates.xyz).

5. Photophysical properties and stability test

UV/vis absorption spectra were recorded on a Shimadzu UV-3510 spectrometer with a resolution of 0.5 nm. Emission spectra were measured with an FP-6600 Hitachi spectrometer with a resolution of 0.2 nm. Absolute fluorescence quantum yields were determined with a Hamamatsu C9920-02 calibrated integrating sphere system.

Light and solvent precautions. Compound **4** was unchanged for several days in the CHCl_3 solution shielded from light using aluminum foil (Figure S27A), but slowly decomposed under light (Figure S27B). The decomposition rate was accelerated under the diluted solution (1×10^{-5} M, Figure S27C). When exposed to ambient light, the CHCl_3 solution of the product tended to turn yellowish, indicating undesirable decomposition processes. The strong fluorescence spectrum in CHCl_3 solution is from its decomposed products. Although decomposition seems relatively slow at high concentration, manipulations involving the product was performed shielding the glassware with aluminum foil as much as possible. Furthermore, the product decomposes more slowly in CH_2Cl_2 solution. **Heat precautions.** Compound **4** was slowly decomposed at 100°C in the $\text{CHCl}_2\text{CHCl}_2$ solution shielded from light using aluminum foil in the dark (5×10^{-3} M, Figure S27D). The solid-state compound can be stored for more than two weeks in the dark without decomposition.

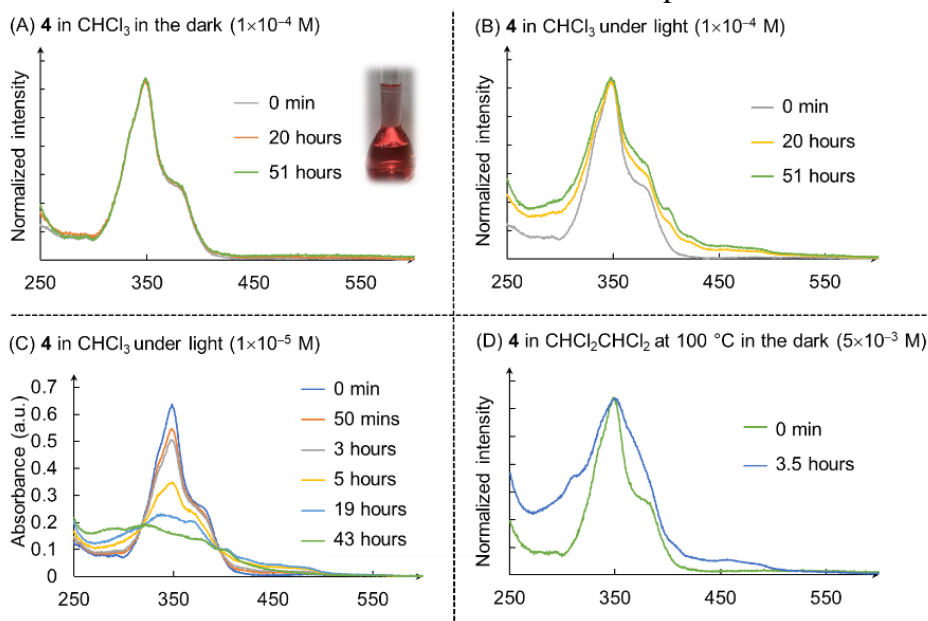


Figure S27. (A) UV/vis absorption spectra of **4** in CHCl_3 in the dark. Inset: the photo of **4** in CH_2Cl_2 ; concentration: 4.7×10^{-4} M (2.5 mg **4** in 10.0 mL CH_2Cl_2). (B–D) UV/vis absorption spectra of **4** under different conditions.

6. Representative aromatic belts having CPP skeleton

The bottom-up synthesis of aromatic belt with CPP as a backbone has rarely been explored to date. In 2017, our group successfully used ethenylene bridges to connect phenylene units to give a fully fused and conjugated carbon nanobelt.¹¹ Subsequently, Chi, Miao, and coworkers achieved the synthesis of phenylene-bridged carbon nanobelt.¹² Very recently, Tanaka's group prepared the CH₂O-bridged [8]CPP.¹³

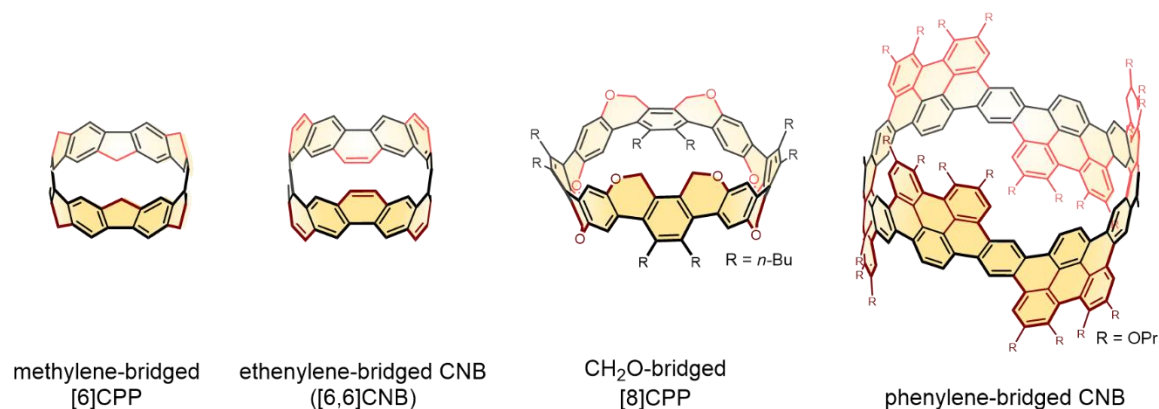
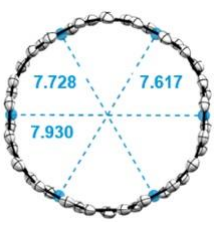
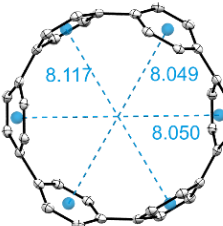
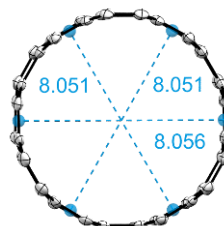
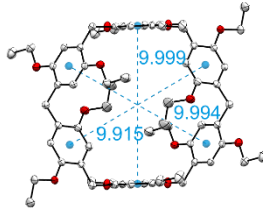
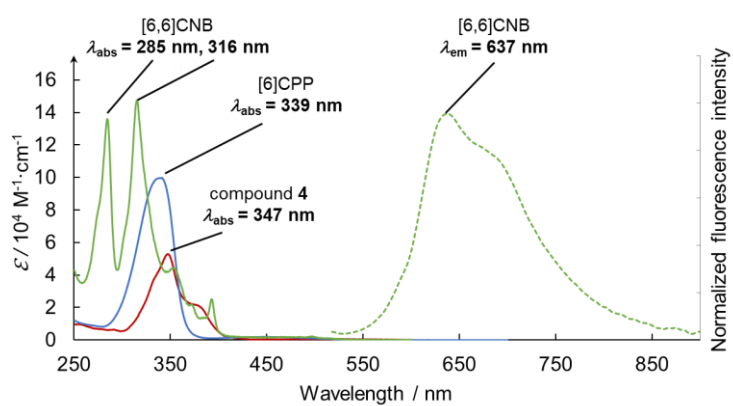
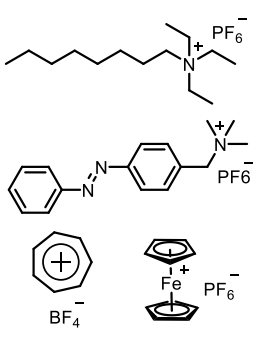


Figure S28. Aromatic belts having CPP skeleton.

7. Comparison among 4, [6]CPP, [6,6]CNB, and pillar[6]arene

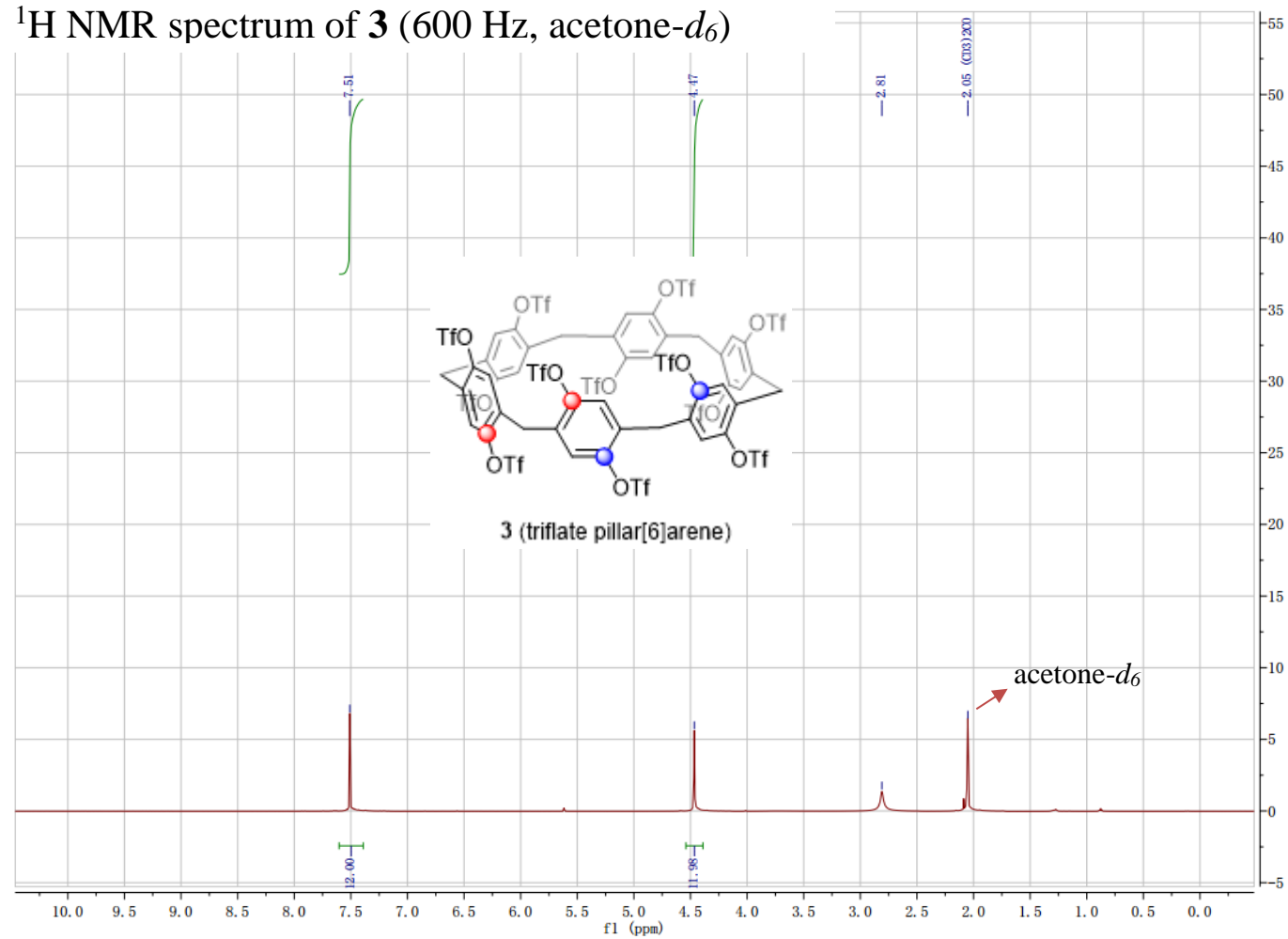
Table S8: Comparison among 4, [6]CPP, [6,6]CNB, and pillar[6]arene.

compound ^a	4	[6]CPP	[6,6]CNB	pillar[6]arene
structure				
diameter (Å) ^b	7.758	8.072	8.053	~10.0 ^c
guest	<i>n</i> -hexane, CH ₂ Cl ₂	CHCl ₃ ^c	CHCl ₃ ^d , THF ^d	
C–C (Å) ^e	1.478	1.489	1.464	
HOMO (eV) ^f	–4.40	–4.91	–4.92	
LUMO (eV) ^f	–1.74	–1.78	–1.97	
energy gap (eV)	2.66	3.13	2.95	
<i>E</i> _{1/2} (V) ^g	0.03, 0.19	0.44	–	
strain energy ^h (kcal/mol)	110.2	96.9	119.5	
fluorescence quantum yield ⁱ	–	–	3%	
UV/Fl				 (see more in ref) ¹⁴

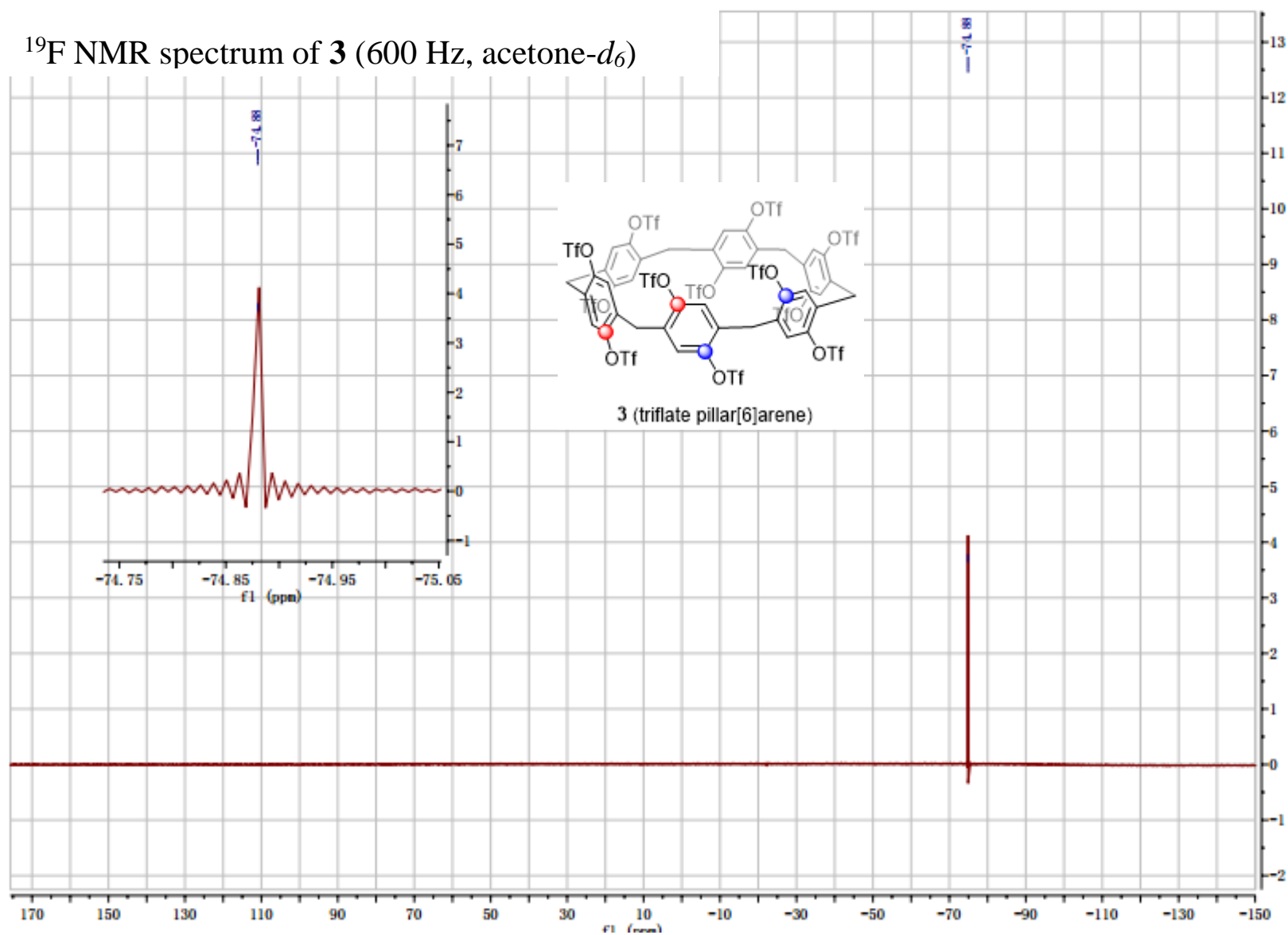
^aThe crystal data of [6]CPP,¹⁵ [6,6]CNB,^{11a} and pillar[6]arene^{14b} were taken from references. ^bThe averaged diameter was measured as the distance between the two central phenylene units located at opposite sides. ^cThe structure shape of pillar[6]arene is hexagon, the diameter of the circle in the hexagon is ~10.0 Å. ^dThe guest molecule was partially incorporated. ^eThe C–C single bond connecting the neighboring phenylene units (the averaged length). ^fFrontier molecular orbitals calculated at the B3LYP/6-31G(d) level of theory. ^gHalf-wave oxidation potential vs Fc/Fc⁺ in Bu₄NPF₆/CH₂Cl₂ solution.¹⁶ ^hThe strain energy data of [6]CPP^{10b} and [6,6]CNB^{11a} were taken from references (calculated at the B3LYP/6-31G(d) level). ⁱThe quantum yield data of [6]CPP¹⁶ and [6,6]CNB^{11a} was taken from references.

8. NMR spectra of new compounds

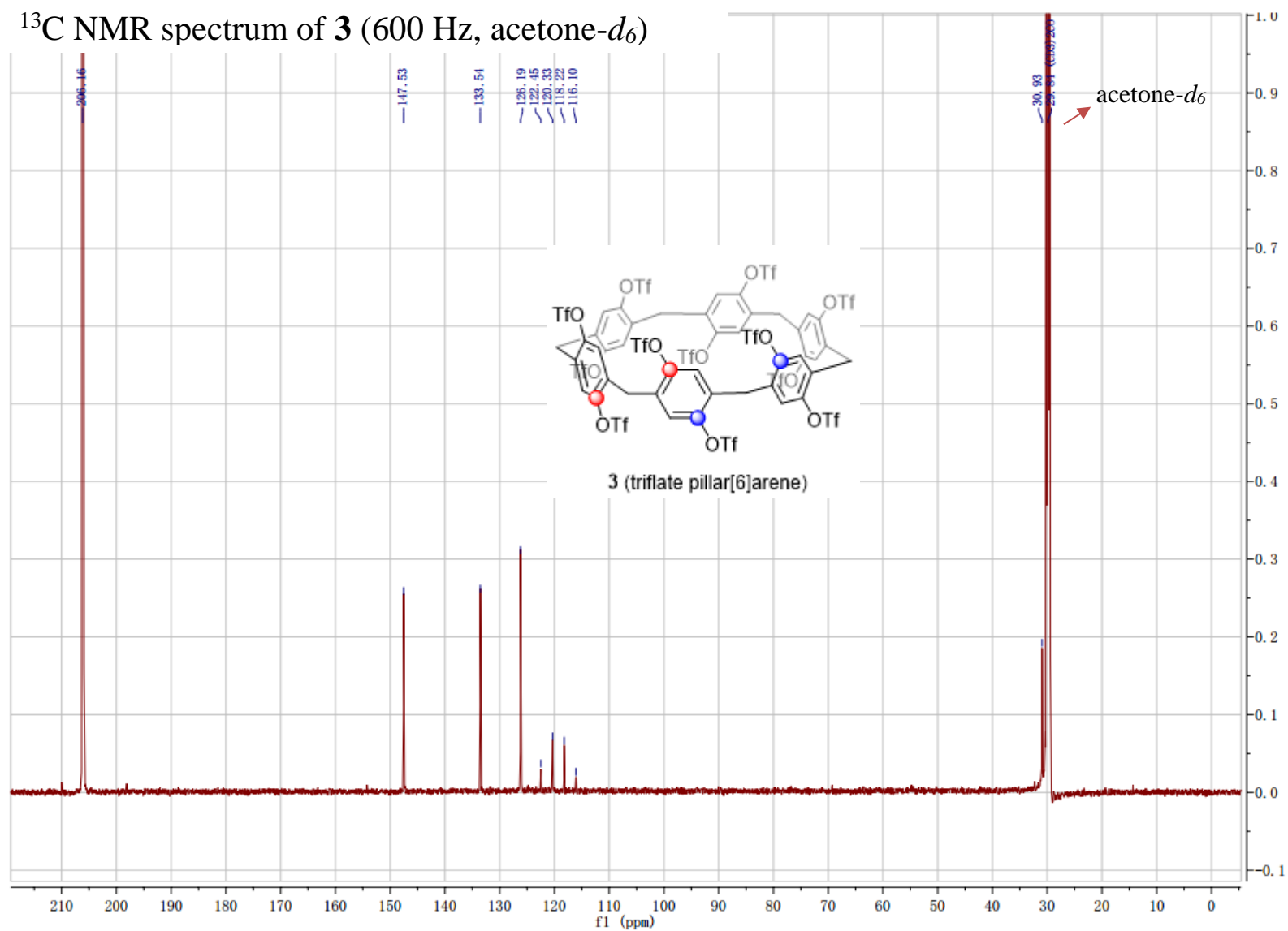
^1H NMR spectrum of **3** (600 Hz, acetone- d_6)



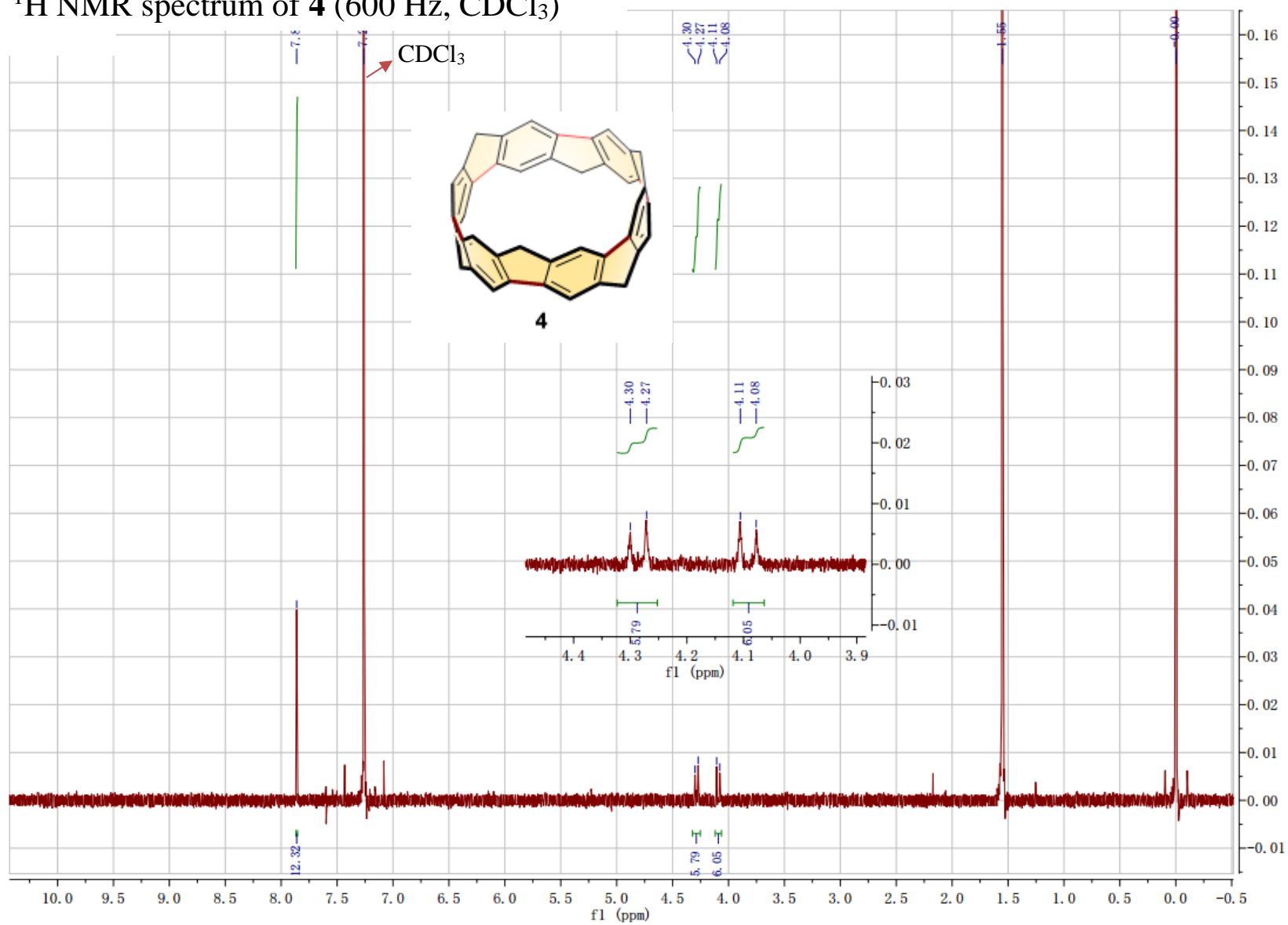
^{19}F NMR spectrum of **3** (600 Hz, acetone- d_6)



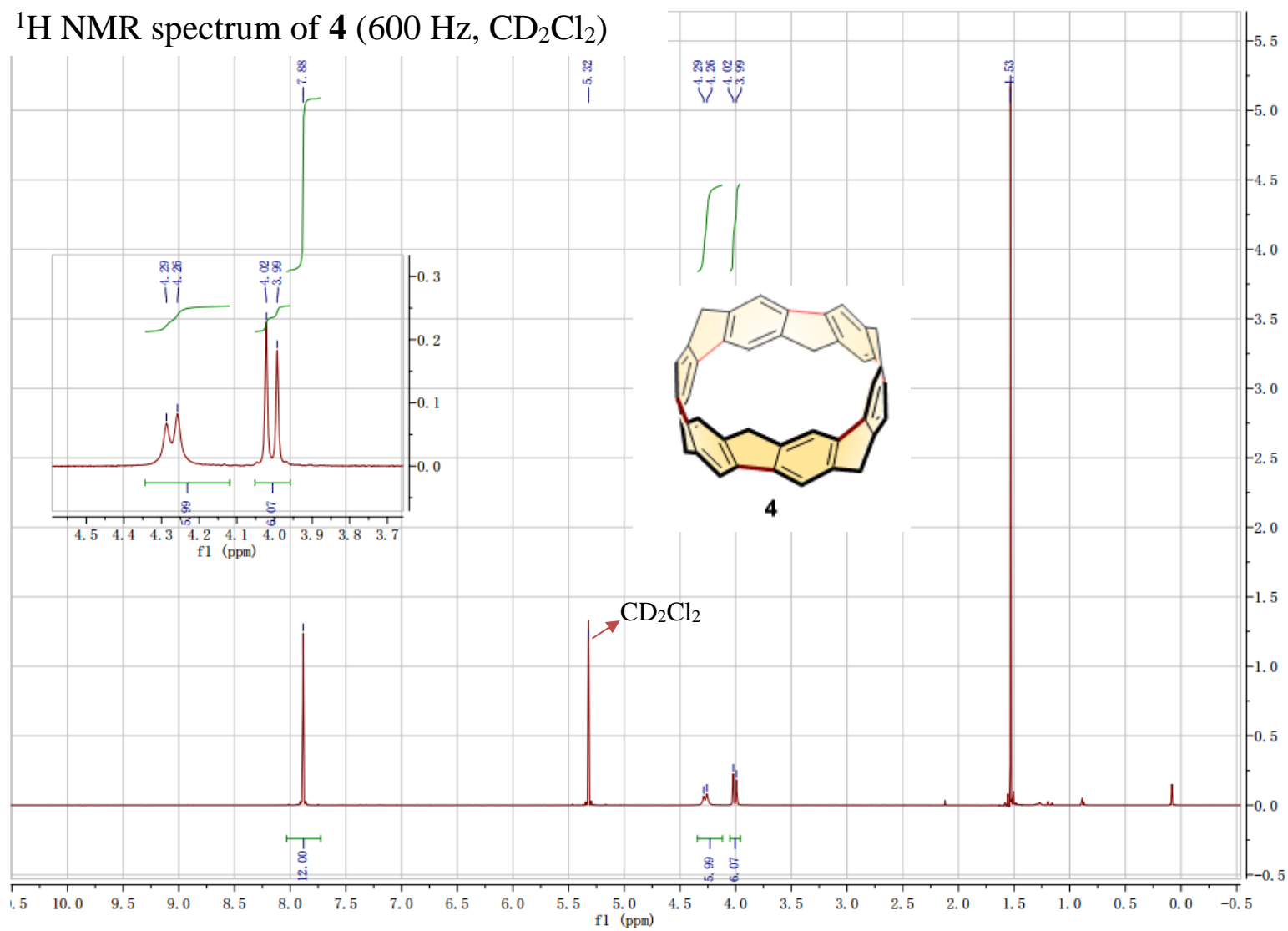
^{13}C NMR spectrum of **3** (600 Hz, acetone- d_6)



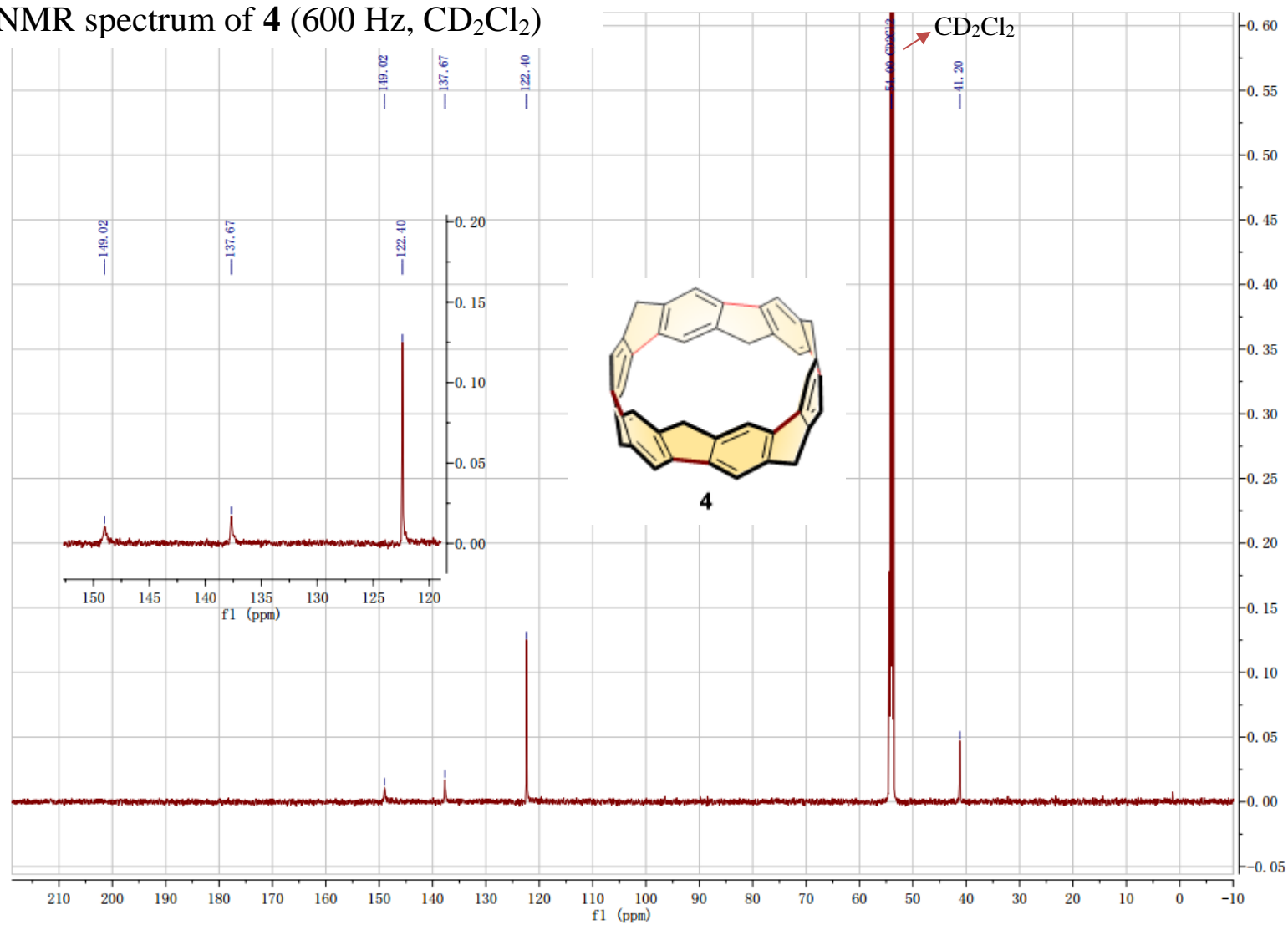
^1H NMR spectrum of **4** (600 Hz, CDCl_3)



^1H NMR spectrum of **4** (600 Hz, CD_2Cl_2)



^1H NMR spectrum of **4** (600 Hz, CD_2Cl_2)



9. References

- (1) Cao, D.; Kou, Y.; Liang, J.; Chen, Z.; Wang, L.; Meier, H. A Facile and Efficient Preparation of Pillararenes and a Pillarquinone. *Angew. Chem., Int. Ed.* **2009**, *48*, 9721–9723.
- (2) Hu, X.-B.; Chen, Z.; Chen, L.; Zhang, L.; Hou, J.-L.; Li, Z.-T. Pillar[n]arenes (n = 8–10) with two cavities: synthesis, structures and complexing properties. *Chem. Commun.* **2012**, *48*, 10999–11001.
- (3) Ma, Y.; Chi, X.; Yan, X.; Liu, J.; Yao, Y.; Chen, W.; Huang, F.; Hou, J.-L. per-Hydroxylated Pillar[6]arene: Synthesis, X-ray Crystal Structure, and Host–Guest Complexation. *Org. Lett.* **2012**, *14*, 1532–1535.
- (4) Wang, G.; Qiang, H.; Guo, Y.-Z.; Yang, J.; Wen, K.; Hu, W.-B. Systematic rim cyano-functionalization of pillar[5]arene and corresponding host–guest property varieties. *Org. Biomol. Chem.* **2019**, *17*, 4600–4604.
- (5) Sheldrick, G. SHELXT - Integrated space-group and crystal-structure determination. *Acta Crystallogr. A* **2015**, *A71*, 3–8.
- (6) Sheldrick, G. Crystal structure refinement with SHELXL. *Acta Crystallogr.* **2015**, *C71*, 3–8.
- (7) Dolomanov, O. V.; Bourhis, L. J.; Gildea, R. J.; Howard, J. A. K.; Puschmann, H. OLEX2: a complete structure solution, refinement and analysis program. *J. Appl. Crystallogr.* **2009**, *42*, 339–341.
- (8) Frisch, M. J.; Trucks, G. W.; Schlegel, H. B.; Scuseria, G. E.; Robb, M. A.; Cheeseman, J. R.; Scalmani, G.; Barone, V.; Petersson, G. A.; Nakatsuji, H.; Li, X.; Caricato, M.; Marenich, A. V.; Bloino, J.; Janesko, B. G.; Gomperts, R.; Mennucci, B.; Hratchian, H. P.; Ortiz, J. V.; Izmaylov, A. F.; Sonnenberg, J. L.; Williams; Ding, F.; Lipparini, F.; Egidi, F.; Goings, J.; Peng, B.; Petrone, A.; Henderson, T.; Ranasinghe, D.; Zakrzewski, V. G.; Gao, J.; Rega, N.; Zheng, G.; Liang, W.; Hada, M.; Ehara, M.; Toyota, K.; Fukuda, R.; Hasegawa, J.; Ishida, M.; Nakajima, T.; Honda, Y.; Kitao, O.; Nakai, H.; Vreven, T.; Throssell, K.; Montgomery Jr., J. A.; Peralta, J. E.; Ogliaro, F.; Bearpark, M. J.; Heyd, J. J.; Brothers, E. N.; Kudin, K. N.; Staroverov, V. N.; Keith, T. A.; Kobayashi, R.; Normand, J.; Raghavachari, K.; Rendell, A. P.; Burant, J. C.; Iyengar, S. S.; Tomasi, J.; Cossi, M.; Millam, J. M.; Klene, M.; Adamo, C.; Cammi, R.; Ochterski, J. W.; Martin, R. L.; Morokuma, K.; Farkas, O.; Foresman, J. B.; Fox, D. J. *Gaussian 16 Rev. C.01*, Wallingford, CT, 2016.
- (9) (a) Becke, A. D. Density - functional thermochemistry. III. The role of exact exchange. *J. Chem. Phys.* **1993**, *98*, 5648 – 5652. (b) Lee, C.; Yang, W.; Parr, R. G. Development of the Colle-Salvetti correlation-energy formula into a functional of the electron density. *Phys. Rev. B* **1988**, *37*, 785–789.
- (10) (a) Segawa, Y.; Yagi, A.; Ito, H.; Itami, K. A Theoretical Study on the Strain Energy of Carbon Nanobelts. *Org. Lett.* **2016**, *18*, 1430–1433. (b) Segawa, Y.; Omachi, H.; Itami, K. Theoretical Studies on the Structures and Strain Energies of Cycloparaphenylenes. *Org. Lett.* **2010**, *12*, 2262–2265.
- (11) (a) Povie, G.; Segawa, Y.; Nishihara, T.; Miyauchi, Y.; Itami, K. Synthesis of a

- carbon nanobelt. *Science* **2017**, *356*, 172–175. (b) Povie, G.; Segawa, Y.; Nishihara, T.; Miyauchi, Y.; Itami, K. Synthesis and Size-Dependent Properties of [12], [16], and [24]Carbon Nanobelts. *J. Am. Chem. Soc.* **2018**, *140*, 10054–10059.
- (12) Cheung, K. Y.; Gui, S.; Deng, C.; Liang, H.; Xia, Z.; Liu, Z.; Chi, L.; Miao, Q. Synthesis of Armchair and Chiral Carbon Nanobelts. *Chem* **2019**, *5*, 838–847.
- (13) Nishigaki, S.; Shibata, Y.; Nakajima, A.; Okajima, H.; Masumoto, Y.; Osawa, T.; Muranaka, A.; Sugiyama, H.; Horikawa, A.; Uekusa, H.; Koshino, H.; Uchiyama, M.; Sakamoto, A.; Tanaka, K. Synthesis of Belt- and Möbius-Shaped Cycloparaphenylenes by Rhodium-Catalyzed Alkyne Cyclotrimerization. *J. Am. Chem. Soc.* **2019**, *141*, 14955–14960.
- (14) (a) Ogoshi, T.; Yamagishi, T. Pillar[5]- and pillar[6]arene-based supramolecular assemblies built by using their cavity-size-dependent host–guest interactions. *Chem. Commun.* **2014**, *50*, 4776–4787. (b) Yuan, M.-S.; Chen, H.; Du, X.; Li, J.; Wang, J.; Jia, X.; Li, C. Host–guest complexation of pillar[6]arenes towards neutral nitrile guests. *Chem. Commun.* **2015**, *51*, 16361–16364.
- (15) Spisak, S. N.; Wei, Z.; Darzi, E.; Jasti, R.; Petrukhina, M. A. Highly strained [6]cycloparaphenylene: crystallization of an unsolvated polymorph and the first mono- and dianions. *Chem. Commun.* **2018**, *54*, 7818–7821.
- (16) Xia, J.; Jasti, R. Synthesis, Characterization, and Crystal Structure of [6]Cycloparaphenylene. *Angew. Chem., Int. Ed.* **2012**, *51*, 2474–2476.